



Asprosin aggravates atherosclerosis via regulating the phenotype transformation of vascular smooth muscle cells

Yu Zhao^{a,b}, Zhengkai Wang^a, Yi Chen^a, Min Feng^a, Xinxin Liu^a, Huan Chen^a, Nannan Wang^a, Zhiqi Wang^a, Shifeng Cao^a, Jing Ren^a, Xue Liu^a, Yixiu Zhao^{a,*}, Yan Zhang^{a,*}

^a State Key Laboratory of Frigid Zone Cardiovascular Diseases (SKLFZCD), Department of Pharmacology, State Key Laboratory-Province Key Laboratories of Biomedicine-Pharmaceutics of China, Key Laboratory of Cardiovascular Research, Ministry of Education, College of Pharmacy, Harbin Medical University, Harbin 150081, China

^b Department of Pathophysiology, Province Key Laboratory of Medicine-Food Homologous Resources and Prevention and Treatment of Metabolic Diseases, Basic Medical College, Qiqihar Medical University, Qiqihar 161000, China

ARTICLE INFO

Keywords:

Asprosin
VSMCs phenotype transformation
GPR54 signaling
Atherosclerosis

ABSTRACT

Phenotype transformation of vascular smooth muscle cells (VSMCs) plays an important role in the development of atherosclerosis. Asprosin is a newly discovered adipokine, which is critical in regulating metabolism. However, the relationship between asprosin and phenotype transformation of VSMCs in atherosclerosis remains unclear. The aim of this study is to investigate whether asprosin affects the progression of atherosclerosis by inducing phenotype transformation of VSMCs. We established an atherosclerosis model in ApoE^{-/-} mice and administered asprosin recombinant protein and asprosin antibody to mice. Knocking down asprosin was also as an intervention. Interestingly, we found a correlation between asprosin levels and atherosclerosis. Asprosin promoted plaque formation and phenotype transformation of VSMCs. While, Asp^{KD} or asprosin antibody reduced the plaque lesion and suppressed vascular stiffness in ApoE^{-/-} mice. Mechanistically, asprosin induced phenotype transformation of MOVAs by binding to GPR54, leading to Gαq/11 recruitment and activation of the PLC-PKC-ERK1/2-STAT3 signaling pathway. Si GPR54 or GPR54 antagonist partially inhibited the action of asprosin in MOVAs. Mutant GPR54-(267, 307) residue cancelled the binding of asprosin and GPR54. In summary, this study confirmed asprosin activated GPR54/Gαq/11-dependent ERK1/2-STAT3 signaling pathway, thereby promoting VSMCs phenotype transformation and aggravating atherosclerosis, thus providing a new target for the treatment of atherosclerosis.

1. Introduction

Atherosclerosis is a major health problem worldwide which is an independent risk factor for cardiovascular events, closely related to cardiovascular morbidity and mortality [1]. Clarifying the influencing factors and mechanism of arteriosclerosis is of great significance for further research and development of effective treatment methods. Dysfunctional adipocytes in overweight/obesity conditions lead to unbalanced release of adipokines, which is thought to be a potential link between perivascular adipose tissue (PVAT) and atherosclerosis. It has been proved that adipokines are involved in endothelial function, cholesterol transport, inflammation, immune response, and proliferation, migration of vascular smooth muscle cells, all of which are closely related to the progression of atherosclerosis [2]. However, different

adipokines play different roles in the process of atherosclerosis, some promote and some inhibit the occurrence of atherosclerosis under pathological conditions.

Asprosin, a new adipokine mainly secreted by white adipose tissue. It is the C-terminal cleavage product of profibrillin (encoded by FBN1) [3], which composed of 140 amino acids encoded by exons of the FBN1 gene (exon 65 and 66). The molecular weight is 30 kDa. Olfactory receptor (OR) OLF734 has been proved to be a receptor of asprosin in the liver to promote hepatic gluconeogenesis [4]. Asprosin has been found to be associated with a variety of clinical diseases, such as diabetes, obesity, polycystic ovary syndrome, coronary heart disease and so on [5]. In 2018, Wang Y et al. found that blood asprosin level was higher in patients with impaired glucose regulation and type 2 diabetes than in healthy controls. They injected asprosin antibody into 16-week-old male

* Corresponding authors at: Harbin Medical University, No.157 Baojian Road, Nangang District, Harbin, Heilongjiang Province, China.

E-mail addresses: zhaoyixiu520@126.com (Y. Zhao), zhangyan@ems.hrbmu.edu.cn (Y. Zhang).

<https://doi.org/10.1016/j.ijbiomac.2024.131868>

Received 9 March 2024; Received in revised form 22 April 2024; Accepted 23 April 2024

Available online 25 April 2024

0141-8130/© 2024 Elsevier B.V. All rights reserved.

diet-induced obesity (DIO) mice, and detected plasma insulin and triglyceride levels 24 h after treatment and found that the treatment of asprosin monoclonal antibody significantly reduced plasma triglyceride levels [6]. It has been reported that the level of serum asprosin in T2DM patients with carotid plaques is significantly higher than in healthy controls, suggesting that asprosin might play a role in the occurrence and development of carotid plaques in T2DM [4]. As a multi target risk factor, whether asprosin can act on arteries and affect the process of atherosclerosis, there are currently no reports.

Vascular smooth muscle cells (VSMCs) are the main cell group that constitutes the middle membrane of arterial blood vessels, which controls vascular tone and blood pressure [7]. The proliferation and migration of VSMCs is pivotal for neointima formation, which lead to vascular remodeling, followed by atherosclerosis progression [8]. Under normal conditions, VSMCs exhibit a static and contractile phenotype in the media of the artery [9]. In response to vascular injury and other stimuli, such as growth factors, platelet-derived growth factors (PDGFs), VSMCs proliferate and migrate to the inner lining of the artery. During this process, VSMCs undergo a phenotypic transformation from the contractile phenotype to a synthetic phenotype, which leads to the formation of new intima of arterial blood vessel and participates in the occurrence and development of atherosclerosis [10,11]. Herein, this current work was performed to identify the role of asprosin on the phenotype transformation of VSMCs in atherosclerosis and explore the potential molecular mechanism.

2. Materials and methods

2.1. Study population

All experimental procedures were approved by the Ethic Committees of Harbin Medical University (approval No. IRB3001619). The study population consisted of 18 healthy individuals and 27 patients diagnosed with coronary atherosclerosis, and all of whom provided written informed consent.

From January 2023 to May 2023, the participants were consecutively recruited. The inclusion criteria include: (1) Atherosclerotic patients diagnosed with plaque formation using coronary ultrasonography and coronary angiography. (2) Patients have complete clinical characteristics. (3) Age is from 35 to 70 years old. The exclusion criteria include: (1) Patients with previous myocardial infarction and percutaneous coronary intervention. (2) Patients with hyperglycemia. (3) Uncontrolled malignant arrhythmia. (4) Patients with severe liver and kidney diseases. The healthy subjects who received for annual routine physical examination in The Second Affiliated Hospital of Harbin Medical University were enrolled in the healthy control group. The healthy control and patient groups were matched for age, sex, and body mass index (BMI). Blood samples were obtained from the two groups and were centrifuged at 1000 \times g for 15 min to collect the plasma.

2.2. Animals and treatment

Wild-type C57BL/6 J mice (male, eight weeks old) and ApoE^{-/-} mice (male, eight weeks old) were purchased from Beijing vital river laboratory animal technology co., Ltd. C57BL/6 J mice were fed with normal diet (ND, Beijing Keao Xieli Feed Co.,Ltd.), ApoE^{-/-} mice were fed with high fat diet (HFD, Beijing Keao Xieli Feed Co.,Ltd.) consisting of 1.25 % cholesterol and 20 % fat for consecutive 18 weeks. Our experiments were approved by the Ethic Committees of Harbin Medical University. ApoE^{-/-} mice were fed with high fat diet (HFD) and were randomly divided into ApoE^{-/-} model group, (ApoE^{-/-} + Asprosin) group, (ApoE^{-/-} + IgG) group and (ApoE^{-/-} + Asprosin antibody) treatment group. The concentration of recombinant mouse asprosin is 7.78 μ g \cdot kg⁻¹, the concentration of IgG and asprosin antibody is 15.56 μ g \cdot kg⁻¹, all three reagents are injected through the tail vein, once a week.

2.3. Cell culture

The MOVAs were obtained from Otwo Biotech (Shenzhen, China) and maintained in Dulbecco's Modified Eagle's Medium (DMEM) supplemented with 10 % fetal bovine serum (Gibco, New Zealand) and 1 % penicillin and streptomycin. The cells were incubated at 37 °C in a 5 % CO₂ humidified atmosphere. LO2 cells were purchased from Shanghai Zhong Qiao Xin Zhou Biotechnology (Shanghai, China). Specific treatment duration and agent concentrations were specified in the corresponding figures or legends.

2.4. The co-culture of WAT explants and VSMCs

Humanely euthanize the mouse via cervical dislocation. Sterilize the abdominal region with 70 % ethanol. Make an incision in the abdomen to expose the internal organs. Using sterile scissors and forceps, harvest the subcutaneous and epididymis adipose tissue. Rinse each collected tissue with phosphate-buffered saline (PBS) supplemented with 1 % antibiotic solution. Gently place the adipose tissue into the upper level of the transwell chamber containing 2 ml of DMEM/F12 medium. Ensure that the explants are fully immersed in the medium. MOVAs is inoculated in the lower layer of transwell chamber. Place the co-culture dishes with the adipose tissue explants in a cell culture incubator set to 37 °C and 5 % CO₂ for 24 h.

2.5. Cell viability

MOVAs were seeded in 96-well plates, cultured to 70 %–80 % confluence and starved for 12 h with 1 % serum culture medium. Cells were incubated with 40 ng/ml PDGF-BB (GenScript, Nanjing, China) or asprosin of different concentrations for 24 h, then 10 μ l CCK8 (North kernel chemical, Beijing, China) working solution was added to each sample and then incubated for 2 h. Absorbance at 450 nm were detected by optical density (OD) by enzyme standard instrument (SYNERGY/HTX, USA).

2.6. EdU

Cell proliferation was detected using the EdU cell proliferation assay Kit (BIO-RAD, USA). To summarize, cells were incubated with 50 μ M EdU for 2 h, fixed with 4 % paraformaldehyde for 30 min and then treated with penetrant (0.5 % TritonX-100) for 10 min. Nuclear DNA was stained with Hoechst 33342 for 30 min, then the images were captured by fluorescence microscope (Olympus, Japan). The numbers of EdU positive cells were calculated by Image J.

2.7. Flow cytometric analysis

Cell cycle distribution was measured using the 7-AAD cell cycle assay kit (4 A Biotech, Beijing, China) as instructed by the manufacturer. The cells were harvested by trypsin and fixed in 95 % ethanol for 12 h–24 h. The cells were washed in PBS and incubated with the 7-AAD staining solution at 37 °C for 30 min, and then the cell cycle distribution was detected by flow cytometry (Agilent, USA). The distribution of G1, S and G2 phase was detected by Novo Express software.

2.8. Wound scratch assays

VSMCs migration was detected by wound scratch assays. Briefly, the VSMCs were seeded in a 6-well plate, cultured to 70 % confluence. After starving for 12 h in 1 % serum culture medium, wounds were scratched to the cell layer by a 200 μ l pipette tip. The images for wound healing were pictured at 4 \times magnification with a light microscope (Olympus, CKX41) at indicated time points.

2.9. Phalloidin staining

Cells were fixed with 4 % paraformaldehyde, permeabilized in 0.5 % Triton X-100 and incubated with 100 nM phalloidin-TRITC for 30 min at room temperature in dark, nuclei were stained with DAPI. Pictures were captured by confocal microscope (Olympus, Japan).

2.10. Collagen content assay

After 24 h of cell culture, MOVAs were treated with recombinant mouse asprosin (100 ng/ml) for 24 h. The control group and asprosin treatment group separately added 200 μ l of cold isolation concentration reagent, and mixed upside down. Half of the EP tube was placed in the ice-water mixture and incubated for 48 h. Samples were removed from the ice-water mixture to avoid shaking and centrifuged at 13800 g for 10 min. Transparent hydration precipitation was visible after centrifugation, carefully discard 1000 μ l of supernatant, the remaining 200 μ l sample was left in the 1.5 ml EP tube. Add 1 ml Sircol Dye Reagent to each tube and mixed slowly manually upside down. Then 750 μ l of pre-cooled acid-salt wash reagent is added to each tube for the purpose of removing unbound dyes from precipitate surfaces and inside the tube. Centrifuge it at 13800 g for 10 min, discard the supernatant and remove the excess dye on the lid and edge. 250 μ l of Alkali Reagent were added to each tube, which could dissolve the precipitation. 200 μ l sample was taken into the 96-well plate and OD value was detected at 555 nm.

2.11. Nuclear and cytoplasmic protein extracting assay

The nuclear proteins and cytoplasmic proteins of cells were extracted and separated by using Nuclear and Cytoplasmic Protein Extraction Kit (Beyotime P0028, China) as previously described [12].

2.12. Surface plasmon resonance (SPR)

The activator is prepared by mixing 400 mM EDC and 100 mM NHS immediately prior to injection. The CM5 sensor chip is activated for 420 s with the mixture at a flow rate of 10 μ l/min. Dilute asprosin to 10 μ g/ml in immobilization buffer, then injected to sample channel (Fc4) at a flow rate of 10 μ l/min, and typically result in immobilization levels of 570 RU, the reference channel (Fc3) does not need ligand immobilization step. The chip is deactivated by 1 M Ethanolamine hydrochloride at a flow rate of 10 μ l/min for 420 s. Dilute GPR54 with the same analyte buffer to 6 concentrations (400, 200, 100, 50, 25 and 0 nM). GPR54 is injected to channel Fc3- Fc4 at a flow rate of 30 μ l/min for an association phase of 120 s, followed by 300 s dissociation. The association and dissociation process are all handling in the analyte buffer. Repeat 6 cycles of analyte according to analyte concentrations in ascending order. After each cycle of interaction analysis, the sensor chip surface should be regenerated completely with 10 mM Glycine-HCl as injection buffer at a flow rate of 30 μ l/min for 30 s to remove the analyte, then next concentration cycle of the analyte GPR54 need to repeat injection and regeneration steps.

2.13. Co-immunoprecipitation

To determine the interaction between proteins, Pierce™ CO-Immunoprecipitation Kit (Thermo fisher, America) was used. Briefly, after 24 h of cell culture, MOVAs were treated with recombinant mouse asprosin (100 ng/ml) for 24 h. Briefly, cells were treated with IP lysis buffer to lytic cells, then we adopted BCA Protein Assay Kit to measure protein concentration and 2 mg cell lysis solution for pre-cleaning. After that, antibodies were immobilized with Amino Link Plus coupling Resin, 15 μ g of His-asprosin antibody or GPR54 antibody were used, coupling buffer and ddH₂O were added, each reaction system was 200 μ l, incubated on a rotary for 120 min, and then resin was washed with washing buffer for 4 times. Then, the pre-cleaning cell lysate was added to the

centrifuge column with fixed antibody, with a total sample volume of 100 μ l–500 μ l, incubated overnight at 4 °C, after 3 times washing, 10 μ l elution buffer was added for centrifugation, and 50 μ l elution buffer was added for further elution. The collected co-immunoprecipitation products were measured by BCA Protein Assay Kit for protein concentration, followed by western blot experiments.

2.14. Duolink in situ assay

Duolink In Situ kits were used to detect the close proximity of asprosin and GPR54 in the experiment. Briefly, after 24 h of cell culture, the experimental group cells were treated with recombinant mouse asprosin (100 ng/ml) for 24 h. In the control well, vehicle (ddH₂O) was added. His-tag asprosin antibody is conjugated to the plus probe, the GPR54 antibody is conjugated to the minus probe at 4 °C overnight. The cells in the two experiments were washed with PBS, fixed with 4 % paraformaldehyde, and permeabilized with 0.2 % Triton-X100. Subsequently, the blocking solution in the Duolink In Situ kit was used for 30 min at 37 °C, after which the cells were treated with the two PLA probes for 1 h at 37 °C, Ligation-Ligase solution was added for 30 min at 37 °C, and Amplification-Polymerase solution was added for 100 min at 37 °C. The cells were then stained with DAPI for 15 min, subsequently captured by confocal microscope (Olympus, Japan).

2.15. Molecular docking

Molecular docking was performed to investigate the binding mode between the *mus musculus* GPR54 and the *mus musculus* FBN1 using the ZDOCK server (zdock.umassmed.edu). The three-dimensional (3D) structure of the GPR54 was built by the AlphaFold, while the 3D structure of FBN1 (residues 2732–2871) was obtained by the modeller 9.21. For docking, the default parameters were used as described in the ZDOCK server. The top ranked pose as judged by the docking score was subject to visually analyze using PyMol 1.7.6 software (www.pymol.org).

2.16. Enzyme linked immunosorbent assay

Plasm level of asprosin was determined by enzymelinked immunosorbent assays (ELISA) according the manufacturer's protocol (Finetest, China).

2.17. Adeno-associated virus and viral delivery protocol

To specifically knockdown asprosin in adipose tissue, ApoE^{−/−} mice received a single intraperitoneal injection of adeno-associated virus 8 (AAV8) encoding mouse Fbn1 gene under the hAdipoq mini promoter (AAV8-U6 > (mFbn1-SagRNA)-hAdipoq mini promoter>Kozak-SaCas9). The injected virus was 2.0*10¹¹ GC/ml. The control group was injected with AAV8-CMV-EGFP adeno-associated virus. Adeno-associated virus were generated by Cyagen Biosciences (Guangzhou, China).

2.18. Doppler ultrasound

The ascending aorta is shown 3 cm above the aortic valve, which was imaged from the parasternal long-axis view. In addition, we also examined the section of the aortic arch. Systolic aortic diameter (As) was measured at the end of t wave on ECG, and diastolic aortic diameter (Ad) was measured at the end of p wave on ECG using M-mode echocardiography, these indicators were detected by doppler ultrasound imaging system (VINNO, Suzhou, China). Average values were taken for 3 measurements of diameter used for data analysis. Three elastic indices of aortic stiffness, namely aortic distensibility (D), stiffness index (β), and elastic modulus (Ep), were calculated respectively as $D = 2(As-Ad)/[Ad(Ps-Pd)]$, $\beta = \ln(Ps/Pd)/[(As-Ad)/Ad]$, and $Ep = (Ps-Pd)/[(As-Ad)/Ad]$,

where Ps = systolic blood pressure, Pd = diastolic blood pressure, and \ln = natural logarithm [13].

2.19. HE staining

HE staining kit (Solarbio, China) was used to stain frozen slices of aortic root. In brief, gently rinse the aortic root (10 μ m) with distilled water and dry the surrounding water. Hematoxylin was stained for 8 min, and the floating colour was washed with distilled water. The differentiation solution used to differentiate for 3 min and washed twice with running water for 2 min each time. Frozen slices of aortic root were

placed in eosin solution for 1 min and rinsed with distilled water for 2 min–3 min. Using 75 %, 85 %, 90 %, 95 % and 100 % ethanol soak dehydration, xylene made it transparent, neutral resin used to seal slices. Images were taken by Leica Microsystems (Solms, Germany). Aortic valve lesion areas were calculated by Image J.

2.20. Oil red O staining

Oil red O (Sigma O0625, USA) was used to stain frozen slices of aortic root. Briefly, we used filter paper to soak the frozen section, then immersed in 60 % isopropyl alcohol solution for 20 s, then immediately

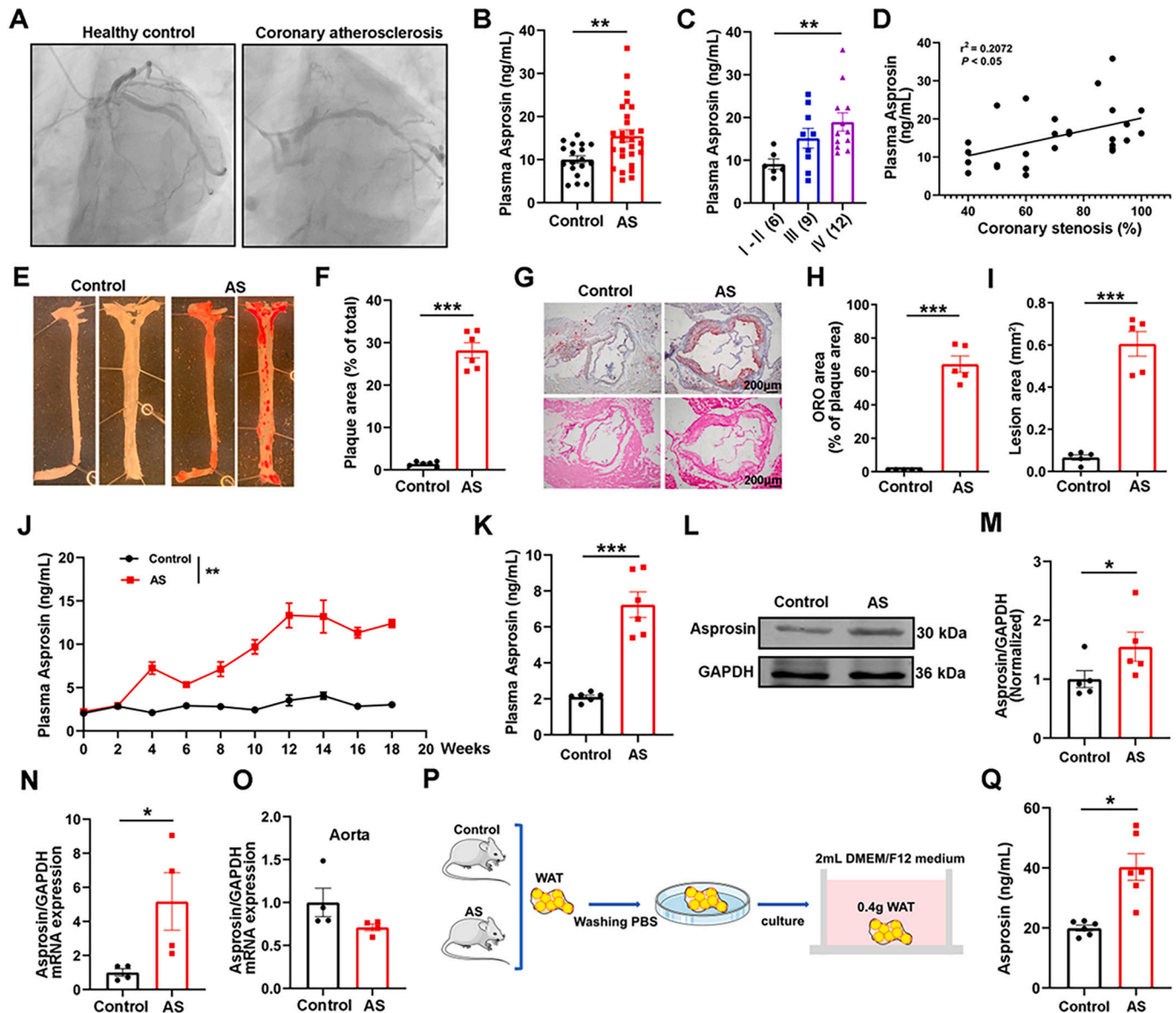


Fig. 1. Asprosin level increases in patients with coronary atherosclerosis and atherosclerosis mice. (A) Representative radiography images of healthy controls and patients with coronary atherosclerosis. (B) Plasma asprosin level in healthy control group and patients with coronary atherosclerosis, control, $n = 18$, AS, $n = 27$, ** $P < 0.01$ vs. Control. (C) Comparison of asprosin level in patients with different stages of coronary artery stenosis in patients with coronary atherosclerosis. ** $P < 0.01$ vs. (I-II stage). (D) Correlation between plasma asprosin level and severity of coronary artery stenosis in patients with coronary atherosclerosis. (E, F) Representative images of aorta Oil red O staining and summarized data of plaque area ratio. $n = 6$, *** $P < 0.001$ vs. Control. (G, H, I) Representative Oil red O and HE staining of aorta root and quantification data. $n = 5$, *** $P < 0.001$ vs. Control. (J) The changes of plasma asprosin level of ApoE^{-/-} mice fed with high fat diet and C57BL/6 J mice fed with normal diet from 0 week to 18 week. $n = 6-10$, ** $P < 0.01$ vs. Control. (K) Plasma asprosin level after C57BL/6 J mice fed with normal diet and ApoE^{-/-} mice fed with high fat diet for 4 weeks. $n = 6$, *** $P < 0.001$ vs. Control. (L, M) The representative western blot and quantification data of adipose asprosin protein levels. $n = 5$, * $P < 0.05$ vs. Control. (N) The mRNA levels of asprosin in adipose, $n = 4$, * $P < 0.05$ vs. Control. (O) The mRNA levels of asprosin in aorta, $n = 4$, $P > 0.05$ vs. Control. (P) Pattern diagram of cultured adipose tissue (epididymis + subcutaneous) explants. (Q) Asprosin level of medium supernatant. $n = 6$, * $P < 0.05$ vs. Control. All data were shown as mean \pm SEM.

put it into the ice-water mixture for 10 s, immersed in Oil red O working liquid staining for 15 min in dark environment. After that, slices were immersed in 60 % isopropyl alcohol solution for 3 s, then immersed in ice-water for 10 s, immersed in Mayer's hematoxylin dye solution (Solarbio, G1080) for 3 min, then used running water to promote it blue for 10 min.

2.21. Masson staining

Masson trichromatic staining Kit (Solarbio, China) was used to stain frozen slices of aortic root. Sections were fixed in 4 % formalin solution for 1 h and then fixed overnight with Davison's fixative solution. The sections were stained with weigert ferric hematoxylin staining solution for 10 min, and treated with the acidic ethanol differentiation solution. Masson blue liquid returns to blue for 4 min, then the slides were stained with ponceaux magenta staining solution. The slices were cleaned with phosphomolybdic acid for 1 min and then washed with the weak acid working solution (distilled water: glacial acetic acid = 1:1) for 1 min. Aniline blue staining for 15 s followed by weak pickling for 1 min. The slices were quickly dehydrated with 95 % ethanol and dehydrated with anhydrous ethanol. Finally, xylene was used for transparent, followed by being sealed in neutral gum. Images were taken by Leica microsystems (Solms, Germany). Aortic valve collagen content was calculated by Image J.

2.22. Immunofluorescence staining

Briefly, the cells and slices were fixed with 4 % paraformaldehyde (Biosharp, China) for 30 min, permeabilized in 0.2 % Triton X-100 (Biosharp, China) +1 % bovine serum albumin (BSA) at room temperature for 15 min, and blocked with 2 % goat serum at room temperature for another 1 h. The cells and slices were incubated with anti- α -SMA (Proteintech, 67,735-1-Ig), anti-OPN (Proteintech, 22,952-1-AP), anti-Asprosin (Biorbyt, orb632871-Biotin) primary antibodies at 4 °C overnight. The secondary antibodies conjugated with Fluorescein (FITC)-conjugated Affinipure Goat Anti-Rabbit IgG (H + L) (Proteintech, SA00003-2) and Rhodamine (TRITC)-conjugated Goat Anti-Mouse IgG (H + L) (Proteintech, SA00007-1) were used to incubate cells for 1 h at room temperature. Finally, Nuclei were counterstained with DAPI (Beyotime, China) for 3 min. Fluorescence was observed under the confocal laser scanning microscope (Olympus, Japan). Fluorescence intensity was calculated by image J.

2.23. The siRNA transfection

All the siRNA were synthesized by RiboBio (Guangzhou, China). The targeting sequences of GPR54 siRNA were 5'-CACTGCATGTCCTACAGCA-3'. The targeting sequences of Gαq/11 siRNA were 5'-TGAACCTGAAGGAGTACAA-3'. The siRNA targeting GPR54 and Gαq/11 was transfected into the MOVAs using X-tremeGENE siRNA Transfection Reagent (4,476,093,001, Roche, Branchburg, New Jersey, USA) according to the instructions from the manufacturer.

2.24. Western blot

To obtain the total protein, tissue or cultured cells proteins were extracted with lysis buffer containing 10 % phosphatase inhibitor and 1 % protease inhibitor solution. Protein samples were obtained by centrifugation (15 min, 17,400 g) at 4 °C. Concentrations of proteins were measured by BCA Protein Assay Kit. Protein samples (70 µg) were separated by 10 % or 12 % SDS-PAGE and transferred to nitrocellulose membranes. Membranes were incubated with antibodies at 4 °C overnight. Membranes were incubated with fluorescence-conjugated secondary antibodies (1:10000 dilution, LI-COR) for 1 h. Western blot bands were quantified by using Odyssey infrared imaging system (LI-COR) and Odyssey v3.0 software.

2.25. Quantitative real-time PCR (qPCR)

Cellular total RNA was extracted by using TRIzol Reagent (Invitrogen, USA) following purified successively by chloroform, precipitated with isopropyl alcohol and washed with 75 % alcohol solution. And then NanoDrop 8000 spectrophotometer (Thermo, USA) was applied to analyze the quantity and quality of RNA solved in DEPC water. The reverse transcription process was performed by using the High Capacity cDNA Reverse Transcription Kit (TOYOBO, Japan). The expression of target genes was measured by quantitative real-time PCR analysis (SYBR® Green Realtime PCR Master Mix, TOYOBO, QPK-201). The relative quantification of target genes was evaluated by using the $2^{-\Delta\Delta CT}$ analytic approach according to an ABI 7500 fast Sequence Detection System (Applied Biosystems). For analysis, GAPDH or β -actin levels were used for normalization.

2.26. Statistical analysis

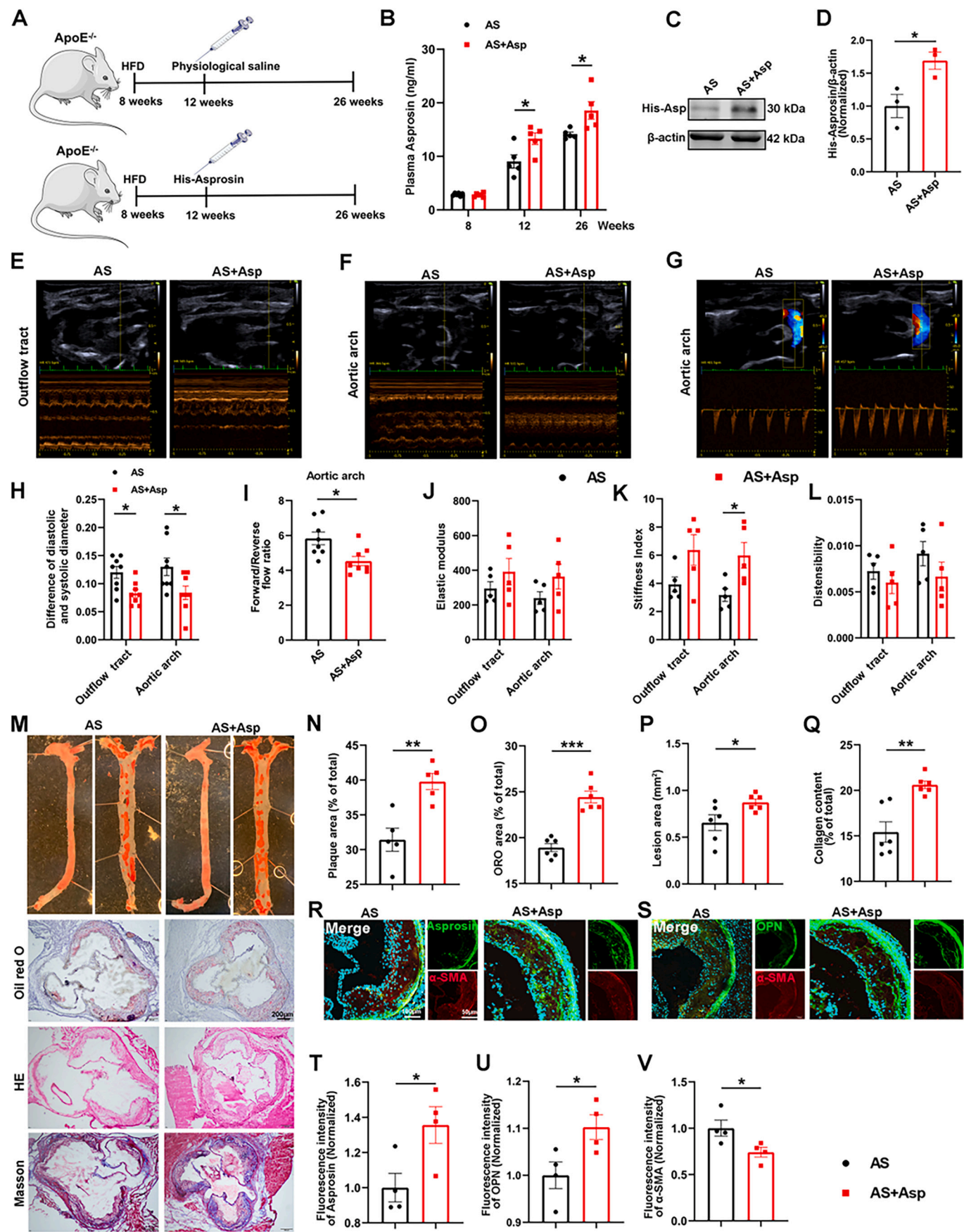
All data are expressed as mean \pm SEM. The Shapiro-Wilk test ($n < 8$) or D'Agostino-Pearson test ($n \geq 8$) was performed to assess data normality. For normally distributed data, we evaluated differences between two groups using two-tailed Student's *t*-test; Two-way analysis of variance (ANOVA) followed by Bonferroni post hoc test was used to compare differences among multiple groups. $P < 0.05$ was considered statistically significant. All statistical analyses were performed using GraphPad Prism version 8.3.0 (GraphPad Software Inc., San Diego, USA).

3. Results

3.1. Asprosin level increases in atherosclerosis patients and mice

To determine the clinical relevance of asprosin and atherosclerosis, we detected the plasma asprosin level from patients with coronary atherosclerosis and compared with healthy people. Coronary angiography technique was used to evaluate atherosclerosis. Representative coronary angiography results in healthy controls and patients with coronary atherosclerosis are shown in Fig. 1A. Table S1 depicted the characteristics of the clinical patients, and there was no significant distinction between them and the healthy controls. Plasma asprosin level of patients with atherosclerosis was significantly higher than that of healthy group (Fig. 1B). According to the degree of coronary artery stenosis, the patients were divided into four grades (I, the area of luminal stenosis <25 %; II, 26 % ~ 50 %; III, 51 % ~ 75 %; IV, 76 % ~ 100 %). We found that the plasma asprosin level was positively correlated with the severity of coronary artery stenosis (Fig. 1C, D). These results indicate that asprosin is related to the development of atherosclerosis.

In order to further clarify the concentration changes of asprosin in atherosclerosis progression, ApoE^{-/-} mice were fed with high fat diet for 18 weeks, we found that body weight of model mice was higher than control group (Fig. S1A). Atherosclerotic plaques in the aorta and aortic root were evaluated by oil red O, HE and masson staining. The results of oil red O staining showed that the plaques of AS model mice were significantly larger than those of control group (Fig. 1E, F). Aortic root Oil red O staining and HE staining suggested AS model mice developed significant lipid deposits and plaque formation compared with control mice (Fig. 1G, H, I), and masson staining showed that there was more collagen in aortic root of AS model mice (Fig. S1B, C). Plasma was taken every two weeks to detect the level of asprosin. We found that the plasma asprosin level increased gradually with the prolongation of feeding time. Moreover, the plasma asprosin level of model group was significantly higher than that of control group after four weeks (Fig. 1J, K). Circulating asprosin mainly comes from white adipose tissue [14], so asprosin level in white adipose tissue was examined by western blot and PCR. The asprosin level in white adipose tissue of the atherosclerosis



(caption on next page)

Fig. 2. Asprosin exacerbates atherosclerosis. (A) Pattern diagram of tail vein administration of His-asprosin in mice. (B) Plasma asprosin levels at different time points. $n = 5$ or 6 , $^*P < 0.05$ vs. AS. (C, D) Representative western blot and quantification data of His-asprosin protein levels in aorta showed that exogenous asprosin recombinant protein was detected in aorta. $n = 3$, $^*P < 0.05$ vs. AS. (E, F, H) Representative ultrasound images of aortic outflow tract and aortic arch and summarized data of the difference of diastolic and systolic diameter. Asp, Asprosin ($7.78 \mu\text{g}\cdot\text{kg}^{-1}$). $n = 8$, $^*P < 0.05$ vs. AS. (G, I) Representative images of aortic arch flow and analyzed data of forward/reverse flow ratio. $n = 8$, $^*P < 0.05$ vs. AS. (J, K, L) Summarized data of elastic modulus, stiffness index, and distensibility of aortic outflow tract and aortic arch. $n = 5$, $^*P < 0.05$ vs. AS. (M) Representative Oil red O staining of aorta, aorta root and representative HE staining, masson staining of aorta root. (N) Summarized data of Oil red O staining of aorta. $n = 6$, $^{**}P < 0.01$ vs. AS. (O) Summarized data of Oil red O staining of aorta root. $n = 6$, $^{***}P < 0.001$ vs. AS. (P) Summarized HE staining of aorta root and summarized data. $n = 6$, $^*P < 0.05$ vs. AS. (Q) Summarized masson staining of aorta root and summarized data. $n = 6$, $^{**}P < 0.01$ vs. AS. (R, T) Representative immunofluorescence images of asprosin and α -SMA colocalization in aortic root. $n = 4$, $^*P < 0.05$ vs. AS. (S, U, V) Representative immunofluorescence images of OPN and α -SMA double dyeing in aortic root. $n = 4$, $^*P < 0.05$ vs. AS. All data were shown as mean \pm SEM.

model group was significantly higher than that of the control group (Fig. 1L–N). However, there was no difference in the level of asprosin mRNA in the aorta of atherosclerotic mice compared with control mice (Fig. 1O). Since adipose tissue is a secretory organ, we performed *in vitro* culture of adipose tissue. All of the epididymis and subcutaneous white adipose tissue with a total mass of about 0.4 g was obtained from each mouse. 0.4 g adipose tissue was accurately weighed and cultured in 2 ml DMEM/F12 medium. Asprosin level in the supernatant was detected by ELISA (Fig. 1P). The results showed that the adipose tissue of mice in the atherosclerosis model group secreted higher asprosin than the control group (Fig. 1Q). These results indicate that the asprosin level is closely related to the development of atherosclerosis, in the atherosclerosis model, the adipokine asprosin secreted by white adipose tissue and released into the blood increased.

3.2. Asprosin exacerbates atherosclerosis in $\text{ApoE}^{-/-}$ mice

To demonstrate that asprosin promotes atherosclerosis, $\text{ApoE}^{-/-}$ mice were injected through tail vein with recombinant asprosin protein once a week for 14 weeks starting from the 4th week of high-fat diet feeding (Fig. 2A). We detected the plasma asprosin level, as shown in Fig. 2B, we found that plasma levels of asprosin increased after administration of asprosin recombinant protein. Western blot results showed that exogenous asprosin recombinant protein which was detected through His-tag was found in aorta (Fig. 2C, D). These results confirmed the successful injection of exogenous asprosin.

Aortic stiffness is believed to be the earliest detectable manifestation of adverse structural and functional changes within the aortic wall [15]. Therefore, we detected aortic diameter and blood flow by doppler ultrasound to evaluate vascular stiffness. Recombinant asprosin treatment significantly reduced the difference of diastolic and systolic diameter in aortic outflow tract and aortic arch (Fig. 2E, F, H). It has been reported aortic sclerosis resulting in reversal of aortic blood flow [16], so we examined aortic flow reversal (ie, retrograde flow from the descending thoracic aorta toward the aortic arch), namely aortic arch forward/reverse flow ratio. We found that recombinant asprosin significantly reduced the forward/reverse flow ratio, indicating asprosin increased reverse flow (Fig. 2G, I). Combined with blood pressure data (Table S2), we got three indicators for evaluating aortic stiffness, namely elastic modulus (Ep), stiffness index (β), and aortic distensibility (D). Recombinant asprosin has been found to increase the stiffness index of the aortic arch (Fig. 2J–L). The findings suggest that asprosin decreases vascular elasticity in $\text{ApoE}^{-/-}$ mice and plays a role in the progression of atherosclerosis. We further examined the effect of asprosin on atherosclerotic plaque formation. Oil red O staining of aorta showed that exogenous asprosin treatment increased the aortic plaque area (Fig. 2M, N). Aortic root plaque lipid deposition and lesion area were evaluated by Oil red O staining and HE staining respectively. As shown in Fig. 2M, O, P, recombinant asprosin treatment promoted plaque formation. Synthetic phenotype VSMCs exhibit high proliferation and migration capacities, and synthesize massive amounts of extracellular matrix (ECM), such as collagen [17]. Collagen content of aortic root was evaluated by masson staining. The results showed that recombinant asprosin significantly increased collagen content (Fig. 2M, Q). Next, we identified the co-localization of asprosin and smooth muscle cell marker α -SMA by

immunofluorescence, and found that the asprosin level increased in the smooth muscle layer by the treatment of exogenous asprosin (Fig. 2R, T). Phenotype transformation of VSMCs is an important process in the development of atherosclerosis, as it enables them to proliferate and migrate to the intima of the vessels, thereby promoting plaque formation [18]. We investigated the effect of asprosin on aortic smooth muscle phenotype transformation in $\text{ApoE}^{-/-}$ mice. The immunofluorescence staining showed that asprosin promoted the expression of synthetic phenotype protein OPN, and inhibited the expression of contractile phenotype protein α -SMA in VSMCs of aortic root (Fig. 2S, U, V).

3.3. Asprosin deficiency in adipose tissue alleviates atherosclerosis

To clarify the important role of asprosin in the occurrence and development of atherosclerosis, at the second week of high-fat feeding, $\text{ApoE}^{-/-}$ mice were intraperitoneally injected with adeno-associated virus to prepare atherosclerosis model mice with adipose tissue specific asprosin knockdown, and they were fed with high fat diet for 10 weeks (Fig. 3A). The adipose tissue asprosin mRNA and protein levels in the Asp^{KD} group were significantly lower than those in the EGFP control group (Fig. 3B–D). The plasma asprosin level in the mice was detected at the 0th and 8th week of high-fat diet feeding, and the results showed that the circulating asprosin level decreased in the Asp^{KD} group (Fig. 3E). Asp^{KD} did not affect blood lipid levels (Fig. S2). Vascular stiffness was evaluated by measuring aortic diameter and blood flow with Doppler ultrasound. Asp^{KD} significantly increased the diastolic and systolic diameter differences of aortic outflow tract (Fig. 3F, I) and aortic arch (Fig. 3G, I). Aortic arch blood flow ultrasound results showed that Asp^{KD} significantly increased the forward/reverse flow ratio (Fig. 3H, J). This suggested that adipose tissue Asp^{KD} partially alleviated vascular dysfunction in atherosclerosis mice. Based on the above aortic diastolic and systolic diameter differences and blood pressure data (Table S3), three indexes for evaluating aortic stiffness were obtained, namely elastic modulus (Ep), stiffness index (β) and distensibility (D). The results showed that Asp^{KD} reduced the aortic stiffness (Fig. 3K–M).

To further explore the effect of Asp^{KD} on atherosclerotic plaque formation, oil red O staining of the aorta showed that Asp^{KD} reduced the aortic plaque area in $\text{ApoE}^{-/-}$ mice (Fig. 3N, Q). Oil red O staining and HE staining were used to evaluate the lipid deposition and lesion area of aortic root, as shown in Fig. 3O, R, S, which indicated that Asp^{KD} inhibited atherosclerotic plaque formation. The results of immunofluorescence showed that Asp^{KD} reduced the localization of asprosin in the smooth muscle layer (Fig. 3P, T). Asp^{KD} reduced the expression of synthetic phenotype protein OPN in aortic root VSMCs and increased the expression of contraction phenotype protein α -SMA (Fig. 3P, U, V). These results suggested that Asp^{KD} inhibited phenotype transformation of VSMCs.

3.4. Asprosin induces the transformation of MOVAs from contractile phenotype to synthetic phenotype

In order to explore whether asprosin induce VSMCs phenotype transformation *in vitro*, given that adipose explants secreted asprosin into the medium in Fig. 1p, we co-cultured white adipose tissues of Control, AS, AS+EGFP and AS+ Asp^{KD} mice with mouse aortic smooth

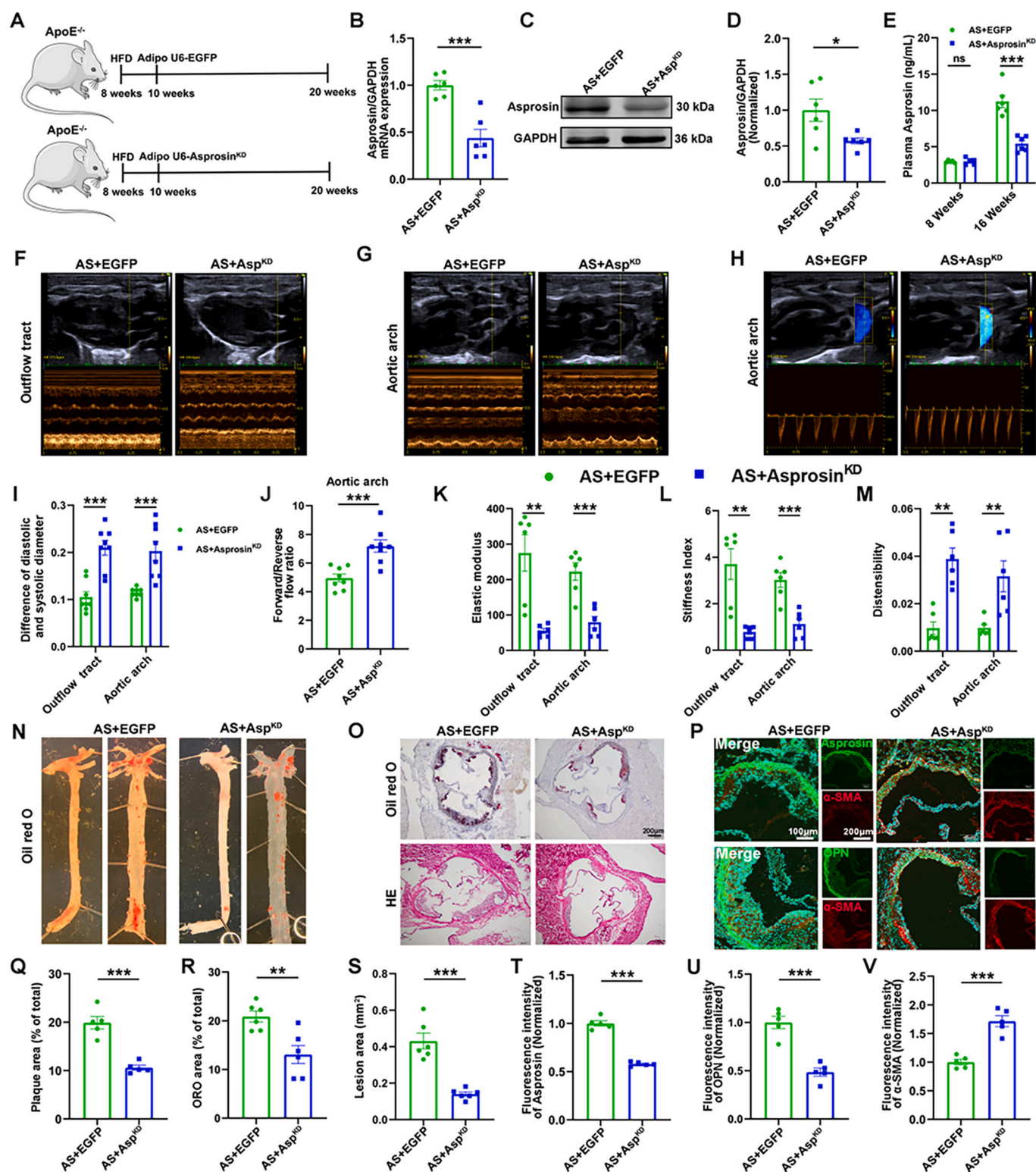


Fig. 3. Asprosin deficiency in adipose tissue alleviates atherosclerosis. (A) Pattern diagram of Asp^{KO} in adipose tissue. (B, C, D) Quantification data of asprosin mRNA and protein levels in aorta. $n = 6$, * $P < 0.05$ vs. (AS+EGFP). *** $P < 0.001$ vs. (AS+EGFP). (E) Plasma asprosin levels at different time points. $n = 6$, *** $P < 0.001$ vs. (AS+EGFP). (F, G, I) Representative ultrasound images of aortic outflow tract and aortic arch and summarized data of the difference of diastolic and systolic diameter. $n = 8$, *** $P < 0.001$ vs. (AS+EGFP). (H, J) Representative images of aortic arch flow and analyzed data of forward/reverse flow ratio. $n = 8$, *** $P < 0.001$ vs. (AS+EGFP). (K, L, M) Summarized data of elastic modulus, stiffness index and distensibility of aortic outflow tract and aortic arch. $n = 6$, ** $P < 0.01$ vs. (AS+EGFP). *** $P < 0.001$ vs. (AS+EGFP). (N, Q) Representative Oil red O staining of aorta and summarized data. $n = 5$, *** $P < 0.001$ vs. (AS+EGFP). (O, R, S) Representative Oil red O staining and HE staining of aorta root and summarized data. $n = 6$, ** $P < 0.01$ vs. (AS+EGFP). *** $P < 0.001$ vs. (AS+EGFP). (P, T, U, V) Representative immunofluorescence images of asprosin and α-SMA colocalization in aortic root. $n = 5$, *** $P < 0.001$ vs. (AS+EGFP). Representative immunofluorescence images of OPN and α-SMA double dyeing in aortic root. $n = 5$, *** $P < 0.001$ vs. (AS+EGFP). All data were shown as mean ± SEM.

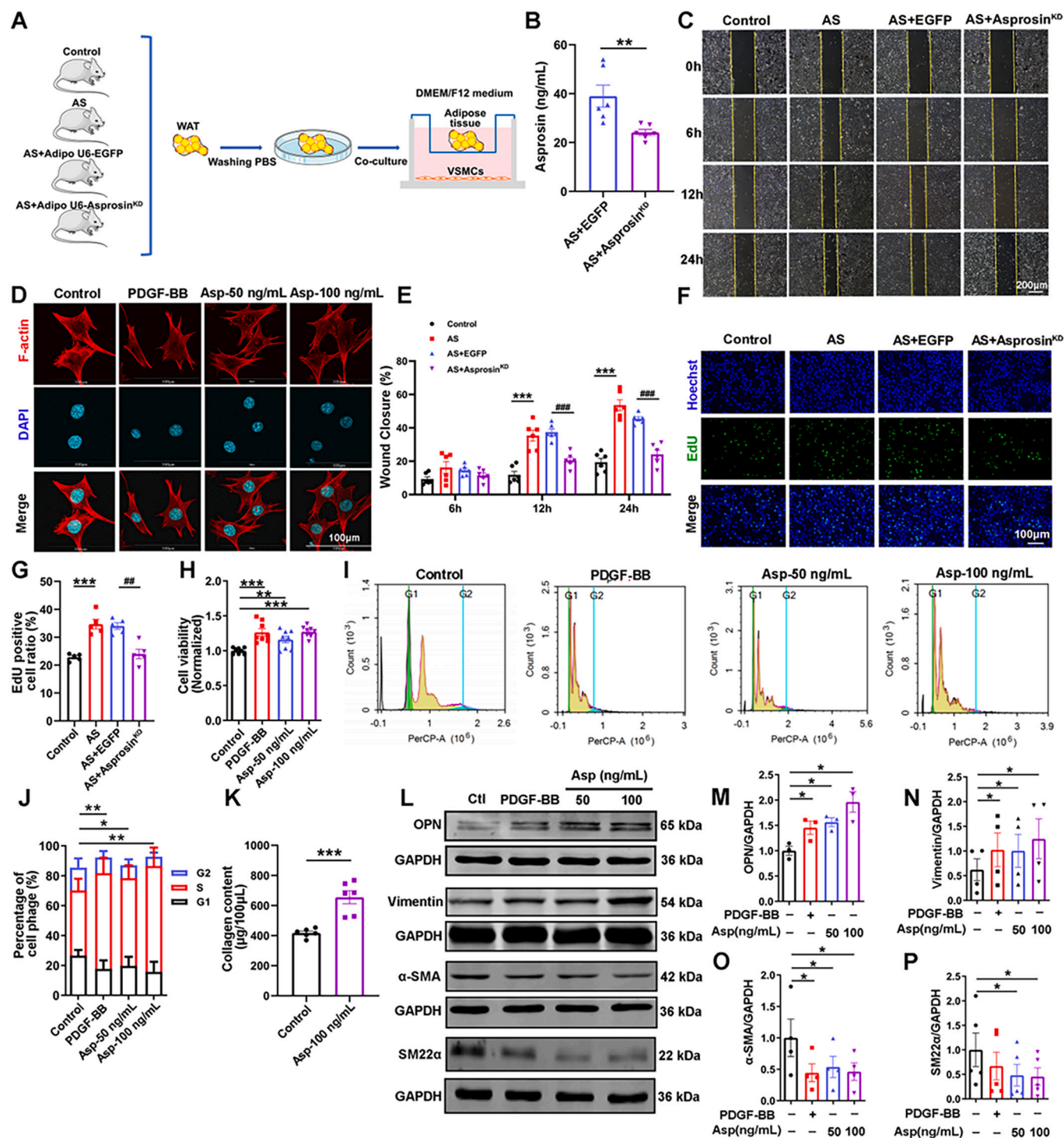
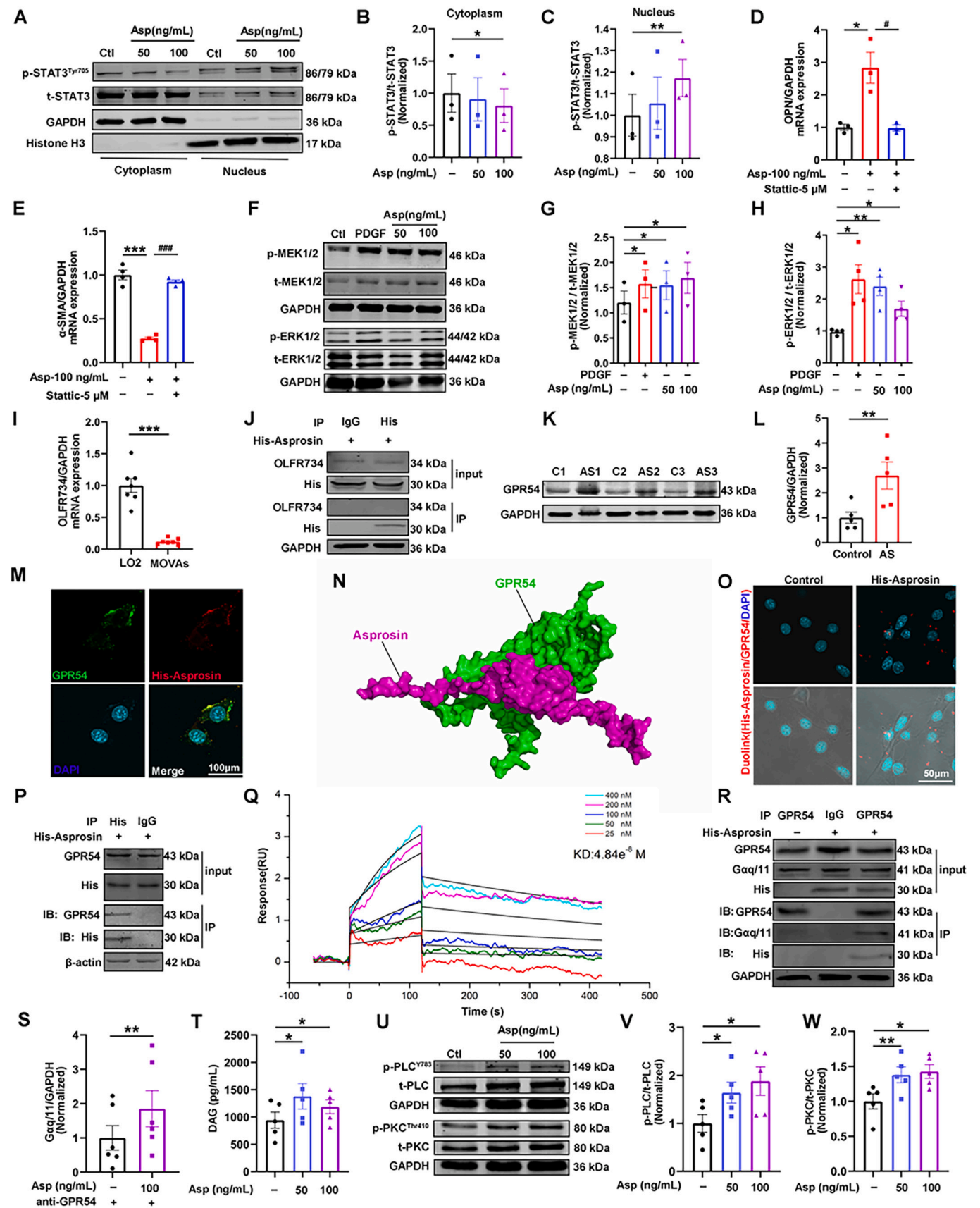


Fig. 4. Asprosin induces the transformation of MOVAs from contractile phenotype to synthetic phenotype. (A) Pattern diagram of the co-culture of adipose tissue (epididymis + subcutaneous) and MOVAs. (B) Asprosin level of medium supernatant. $n = 6$, $**P < 0.01$ vs. (AS+EGFP). (C, E) Representative images of wound scratch assay showed migration of MOVAs induced by adipose at the time 0 h, 6 h, 12 h and 24 h. $n = 6$, $***P < 0.001$ vs. Control. $###P < 0.001$ vs. (AS+EGFP). (D) Representative phalloidin staining of MOVAs treated by PDGF-BB (40 ng/ml) and asprosin (50 ng/ml, 100 ng/ml). (F, G) Representative images and statistical data showed proliferation of MOVAs induced by adipose for 24 h, $n = 5$ in each group. $***P < 0.001$ vs. Control. $##P < 0.01$ vs. (AS+EGFP). (H) Statistical data showed cell viability of MOVAs induced by PDGF-BB (40 ng/ml) and asprosin (50 ng/ml, 100 ng/ml), $n = 8$ in each group. $***P < 0.001$ vs. Control. $**P < 0.01$ vs. Control. (I, J) Representative images and statistical data showed cell cycle of MOVAs induced by PDGF-BB (40 ng/ml) and asprosin (50 ng/ml, 100 ng/ml). $n = 5$. $*P < 0.05$ vs. Control. $**P < 0.01$ vs. Control. All data were shown as mean \pm SEM. (K) Statistical data showed collagen secretion of MOVAs induced by asprosin (100 ng/ml), $n = 6$. $***P < 0.001$ vs. Control. (L) Representative synthetic marker and contractile marker protein of MOVAs treated by PDGF-BB (40 ng/ml) and asprosin (50 ng/ml, 100 ng/ml). (M, N) OPN and Vimentin protein statistical data of MOVAs treated by PDGF-BB (40 ng/ml) and asprosin (50 ng/ml, 100 ng/ml). $n = 3-4$, $*P < 0.05$ vs. Control. (O, P) Contractile marker α -SMA and SM22 α protein statistical data of MOVAs treated by PDGF-BB (40 ng/ml) and asprosin (50 ng/ml, 100 ng/ml). $n = 4-5$, $*P < 0.05$ vs. Control. All data were shown as mean \pm SEM.



(caption on next page)

Fig. 5. Asprosin activates the intracellular PLC-PKC-ERK1/2-STAT3 signaling pathway through GPR54. (A, B, C) Representative and statistical images of nuclear and cytoplasmic p/t-STAT3 protein expression in MOVAs treated by asprosin (50 ng/ml, 100 ng/ml). $n = 3$, $^*P < 0.05$ vs. Control. $^{**}P < 0.01$ vs. Control. (D, E) OPN and α -SMA mRNA quantification data of MOVAs treated by Asprosin (100 ng/ml) with and without Stattic (5 μ M), $n = 3$ or 4 in each group, $^*P < 0.05$ vs. Control. $^{#}P < 0.05$ vs. Asprosin. $^{***}P < 0.001$ vs. Control. $^{###}P < 0.001$ vs. Asprosin. (F, G, H) Representative and statistical images of p/t-MEK1/2, p/t-ERK1/2 protein expression in MOVAs treated by PDGF-BB (40 ng/ml) and asprosin (50 ng/ml, 100 ng/ml). $n = 3-4$, $^*P < 0.05$ vs. Control. $^{**}P < 0.01$ vs. Control. (I) OLF734 mRNA levels in LO2 cells and MOVAs. $n = 7$, $^{***}P < 0.001$ vs. LO2. Data were shown as mean \pm SEM. (J) Co-immunoprecipitation demonstrated that His-Asprosin failed to combine with OLF734 in MOVAs, exogenous His-asprosin dose was 100 ng/ml. The amount of anti-IgG and anti-His-asprosin was 15 μ g. (K, L) Representative and statistical images of GPR54 protein expression in the aorta of mice in control and AS model groups. $n = 5$, $^{**}P < 0.01$ vs. Control. (M) Representative images of GPR54 colocalized with exogenous His-asprosin in MOVAs. (N) The molecular docking demonstrated the interaction between the GPR54 (green) and the asprosin (rose red). (O) Duolink assay demonstrated the combination between GPR54 and His-asprosin in MOVAs, exogenous His-asprosin dose was 100 ng/ml, red fluorescence indicates combination of GPR54 and His-asprosin at cell membrane. (P) Co-immunoprecipitation demonstrated the combination between GPR54 and His-asprosin in MOVAs, exogenous His-asprosin dose was 100 ng/ml. The amounts of anti-His-asprosin and anti-IgG was 15 μ g. (Q) SPR analysis showed the interaction and affinity between asprosin and GPR54. (R, S) Co-immunoprecipitation and its statistical images demonstrated there was more combination between GPR54 and Gaq/11 in MOVAs in the presence of asprosin than the control group. In addition, it demonstrated the combination between GPR54 and His-asprosin. Exogenous His-asprosin dose was 100 ng/ml. The amount of anti-GPR54 and anti-IgG was 15 μ g. $n = 6$, $^{**}P < 0.01$ vs. Control. (T) Statistical images of DAG content in MOVAs when treated with 50 ng/ml and 100 ng/ml asprosin. $n = 5$, $^*P < 0.05$ vs. Control. (U, V, W) Representative and statistical images of p/t-PLC, p/t-PKC protein expression in MOVAs treated by asprosin (50 ng/ml, 100 ng/ml). $n = 5$, $^*P < 0.05$ vs. Control. $^{**}P < 0.01$ vs. Control. All data were shown as mean \pm SEM.

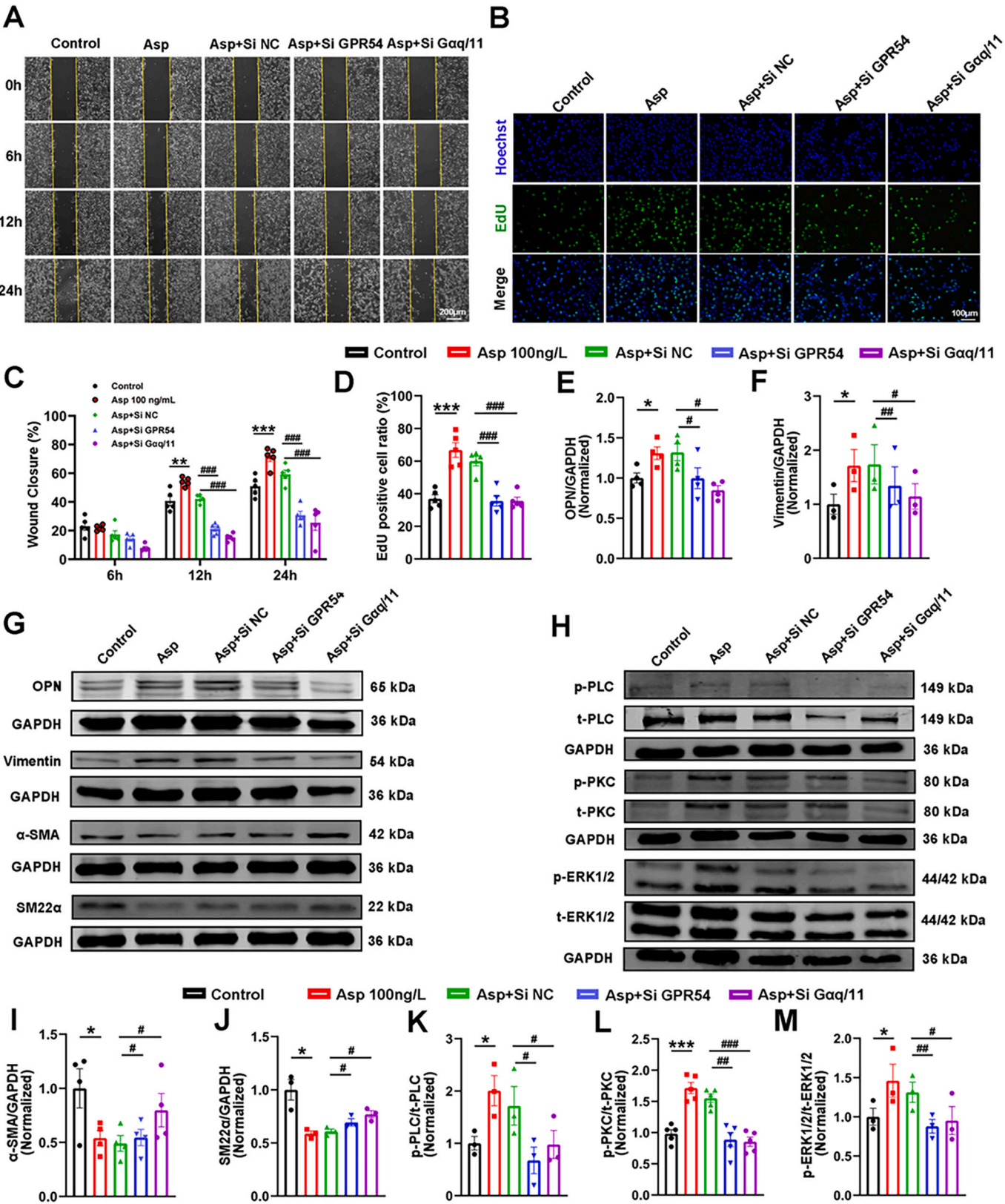
muscle cells, namely MOVAs (Fig. 4A). Asprosin level in the supernatant from (AS+Asp^{KD}) mice was significantly lower than that in the (AS+EGFP) group (Fig. 4B). Co-cultured white adipose tissues from AS promoted cell migration and proliferation than control group (Fig. 4C, E, F, G). However, Asp^{KD} inhibited MOVAs migration and proliferation. Since the establishment of co-culture system requires a large number of mice, asprosin recombinant protein (HY-P7811, MCE, Endotoxin <1 EU/ μ g, determined by LAL method) used to act on MOVAs in the subsequent vitro experiments. MOVAs were divided into control, 50 ng/ml asprosin groups, 100 ng/ml asprosin groups, and 40 ng/ml PDGF-BB as positive control. Wound scratch assays showed that both 50 ng/ml and 100 ng/ml asprosin time-dependently promoted MOVAs migration (Fig. S3A, B). The effect of asprosin on cell proliferation was examined by EdU. Results showed that asprosin increased EdU positive cells (Fig. S3C, D). Phalloidin staining showed that asprosin significantly inhibited the formation of F-actin (Fig. 4D). CCK8 assay showed that asprosin treatment increased cell viability (Fig. 4H). Based on our discovery of asprosin on cell proliferation, we further examined its impact on the cell cycle of MOVAs through flow cytometry. The results demonstrated that asprosin treatment significantly increased the proportion of S-phase MOVAs in the cell cycle, which was similar to the effect of PDGF-BB (Fig. 4I, J). These suggest that the effect of asprosin on the proliferation of MOVAs is related to promoting abnormal cell cycle. Collagen content was also measured in MOVAs, 100 ng/ml asprosin significantly increased collagen secretion (Fig. 4K). These results demonstrate that asprosin can promote migration, proliferation and secretion in MOVAs.

Migration, proliferation and extracellular matrix secretion are the hallmarks of VSMCs transformation from contractile phenotype to synthetic phenotype [19]. Therefore, we detected whether asprosin induced phenotype transformation in MOVAs. As shown in Fig. 4L-N, asprosin treatment increased the expression of synthetic phenotype protein OPN and Vimentin in MOVAs. However, the expression of contractile phenotype protein α -SMA and SM22 α were reduced by asprosin (Fig. 4L, O, P). Immunofluorescence also confirmed the effects of asprosin on phenotype transformation in MOVAs, as shown in Fig. S4A, C, asprosin increased fluorescence intensity of OPN, moreover, it reduced the fluorescence intensity of α -SMA (Fig. S4B, D). The above results indicate that asprosin promotes the phenotype transformation of MOVAs.

3.5. Asprosin activates intracellular ERK1/2-STAT3 signaling pathway via GPR54/Gaq/11

Next, we attempted to explore the mechanism of asprosin induced phenotype transformation of VSMCs. As is well known, STAT3, is one of the critical transcription factors regulating cell proliferation, differentiation, and apoptosis [20], phosphorylation of STAT3 on the 705 site is related to its nuclear translocation [21,22]. Therefore, we explored whether the role of asprosin in inducing phenotype transformation of

VSMCs was related to STAT3. In our experiments, asprosin treatment promoted nuclear translocation of phosphorylated STAT3 in MOVAs (Fig. 5A-C). We treated MOVAs with STAT3 inhibitor Stattic and found that the increase of OPN gene and the decrease of α -SMA gene induced by asprosin were inhibited (Fig. 5D, E). We then tried to find the regulators of STAT3, as is well known, ERK signaling cascade can affect a variety of cellular functions, such as proliferation, apoptosis, and migration [23], activation of ERK may lead to phosphorylation of STAT3 [24]. Our results in MOVAs validated this intracellular signaling processes. PDGF-BB induces migration and proliferation of VSMCs by activating MEK/ERK signaling cascade [25]. We used 40 ng/ml PDGF-BB as a positive control for activating MEK/ERK signaling. The treatment of asprosin was similar to that of PDGF-BB, which increased phosphorylation of MEK1/2 and ERK1/2 in MOVAs (Fig. 5F-H). The above results indicated asprosin induced phenotype transformation through the ERK1/2-STAT3 signaling pathway. How does asprosin initiate intracellular signaling? It has been proved that liver is the major target organ of asprosin [3]. Li et al. proved that the olfactory receptor OLF734 was a receptor for asprosin and played a key role in glucose homeostasis during fasting and in obesity [26]. Therefore, we compared OLF734 mRNA level in MOVAs with LO2 cells, the results showed that the mRNA level of MOVAs OLF734 was significantly lower than that of LO2 cells (Fig. 5I). In addition, co-immunoprecipitation experiments confirmed that asprosin failed to bind to OLF734 in MOVAs (Fig. 5J). The above data proves that asprosin induces phenotype transformation of vascular smooth muscle cells is independent of OLF734. Therewith, G protein-coupled receptor 54 (GPR54), a receptor that mediates cell proliferation and migration has been selected as the research target. GPR54 is encoded by the KISS1R gene located on chromosome 19 in humans [27], which is a seven-time transmembrane G protein coupled receptor and belongs to the rhodopsin family. It has been reported that the expression of GPR54 in aortic atherosclerosis plaque of ApoE^{-/-} mice increases significantly with age [28]. Activation of GPR54 contributes to accelerate the progression and instability of atheromatous plaques, leading to plaque rupture [29]. In our experiments, MOVAs pre-infected with scramble small interfering RNA and GPR54 siRNA for 24 h, and then treated with 100 nM KP-10, which is a ligand of GPR54. The GPR54 silencing efficiency was detected by qPCR and western blot (Fig. S5A-C). In the wound scratch assays, 100 nM KP-10 time-dependently induced the increase of MOVAs migration, which was partially inhibited by silencing GPR54 (Fig. S5D, E). Results of EdU assay showed that KP-10 treatment increased EdU positive cells, promoted cell proliferation, which were also partially inhibited by GPR54 siRNA (Fig. S5F, G). These results indicated activation of GPR54 enhances the proliferation and migration of vascular smooth muscle cells. Western blot results showed that the expression of GPR54 protein increased in the aorta of atherosclerosis mice compared with control mice (Fig. 5K, L). Nevertheless, 50 ng/ml and 100 ng/ml asprosin treatment failed to change the expression



(caption on next page)

Fig. 6. GPR54 SiRNA or Gαq/11 SiRNA attenuate asprosin induced phenotype transformation in MOVAs. (A, C) Representative images and statistical data showed migration of MOVAs treated by Asprosin (100 ng/ml), Asprosin+Si NC, Asprosin+Si GPR54 and Asprosin+Si Gαq/11 at the time 0 h, 6 h, 12 h and 24 h measured by wound scratch assays. $n = 5$, $^{**}P < 0.01$ vs. Control. $^{***}P < 0.001$ vs. Control. $^{###}P < 0.001$ vs. (Asprosin+Si NC). (B, D) Representative images and statistical data showed proliferation of MOVAs treated by Asprosin (100 ng/ml), Asprosin+Si NC, Asprosin+Si GPR54 and Asprosin+Si Gαq/11, $n = 5$ in each group, $^{***}P < 0.001$ vs. Control. $^{###}P < 0.001$ vs. (Asprosin+Si NC). (E, F, G) Representative synthetic marker OPN and Vimentin protein and statistical data of MOVAs treated by Asprosin (100 ng/ml), Asprosin+Si NC, Asprosin+Si GPR54 and Asprosin+Si Gαq/11, $n = 3$ or 4 in each group, $^{*}P < 0.05$ vs. Control. $^{#}P < 0.05$ vs. (Asprosin+Si NC). $^{##}P < 0.01$ vs. (Asprosin+Si NC). (G, I, J) Representative contractile marker α-SMA and SM22α protein and statistical data of MOVAs treated by Asprosin (100 ng/ml), Asprosin+Si NC, Asprosin+Si GPR54 and Asprosin+Si Gαq/11, $n = 3$ or 4 in each group, $^{*}P < 0.05$ vs. Control. $^{#}P < 0.05$ vs. (Asprosin+Si NC). (H) Representative p/t-PLC, p/t-PKC, p/t-ERK1/2 protein of MOVAs treated by Asprosin (100 ng/ml), Asprosin+Si NC, Asprosin+Si GPR54 and Asprosin+Si Gαq/11. (K, L, M) The p/t-PLC, p/t-PKC, p/t-ERK1/2 protein statistical data of MOVAs treated by Asprosin (100 ng/ml), Asprosin+Si NC, Asprosin+Si GPR54 and Asprosin+Si Gαq/11, $n = 3$ or 5, $^{*}P < 0.05$ vs. Control. $^{***}P < 0.001$ vs. Control. $^{#}P < 0.05$ vs. (Asprosin+Si NC). $^{##}P < 0.01$ vs. (Asprosin+Si NC). $^{###}P < 0.001$ vs. (Asprosin+Si NC). All data were shown as mean ± SEM.

levels of GPR54 protein in MOVAs (Fig. S6A, B). Can asprosin, as a multi targets risk factor, affects the process of atherosclerosis through GPR54? Then we set up biological experiments to validate this process. The experimental results confirm our conjecture. Immunofluorescence showed the colocalization of exogenous His-asprosin and GPR54 in the cell membrane of MOVAs (Fig. 5M). Molecular docking also demonstrated the interaction between the GPR54 (green) and asprosin (rose red, Fig. 5N). What's more, subsequent experiments verified the interaction between asprosin and GPR54. Duolink and Co-immunoprecipitation assay demonstrated their combination in cell membrane (Fig. 5O, P). SPR demonstrated the KD between asprosin and GPR54 was 48.4 nM (Fig. 5Q). It has been proved that KiSS-1/KiSS-1R activates phospholipase C (PLC) via Gαq/11, PLC activation promotes the hydrolysis of phosphatidylinositol-4,5-bisphosphate, thus producing two "second messengers" inositol-1, 4, 5-trisphosphate (IP3) and diacylglycerol (DAG). DAG leads to the activation of protein kinase C (PKC), ERK1/2, and p38 phosphorylation [30]. In this process, Gαq/11 is the G protein that transmits external information perceived by GPR54 into cells. Our co-immunoprecipitation results showed that exogenous His-asprosin treatment significantly increased the binding quantity of Gαq/11 to GPR54 in MOVAs (Fig. 5R, S). Besides, asprosin increased the level of DAG in MOVAs (Fig. 5T), and activated PLC-PKC (Fig. 5U-W). MAPKs signal cascade is the downstream of PLC-PKC [23,24]. It has been reported that GPR54 activation results in activation of the mitogen-activated protein kinase (MAPKs) extracellular signal-regulated kinase ERK1 and ERK2 [31,32], this is consistent with our findings. These results indicate that asprosin activates intracellular ERK1/2-STAT3 signaling pathway by GPR54 and its coupled Gαq/11.

3.6. GPR54 SiRNA or Gαq/11 SiRNA attenuate asprosin induced phenotype transformation in MOVAs

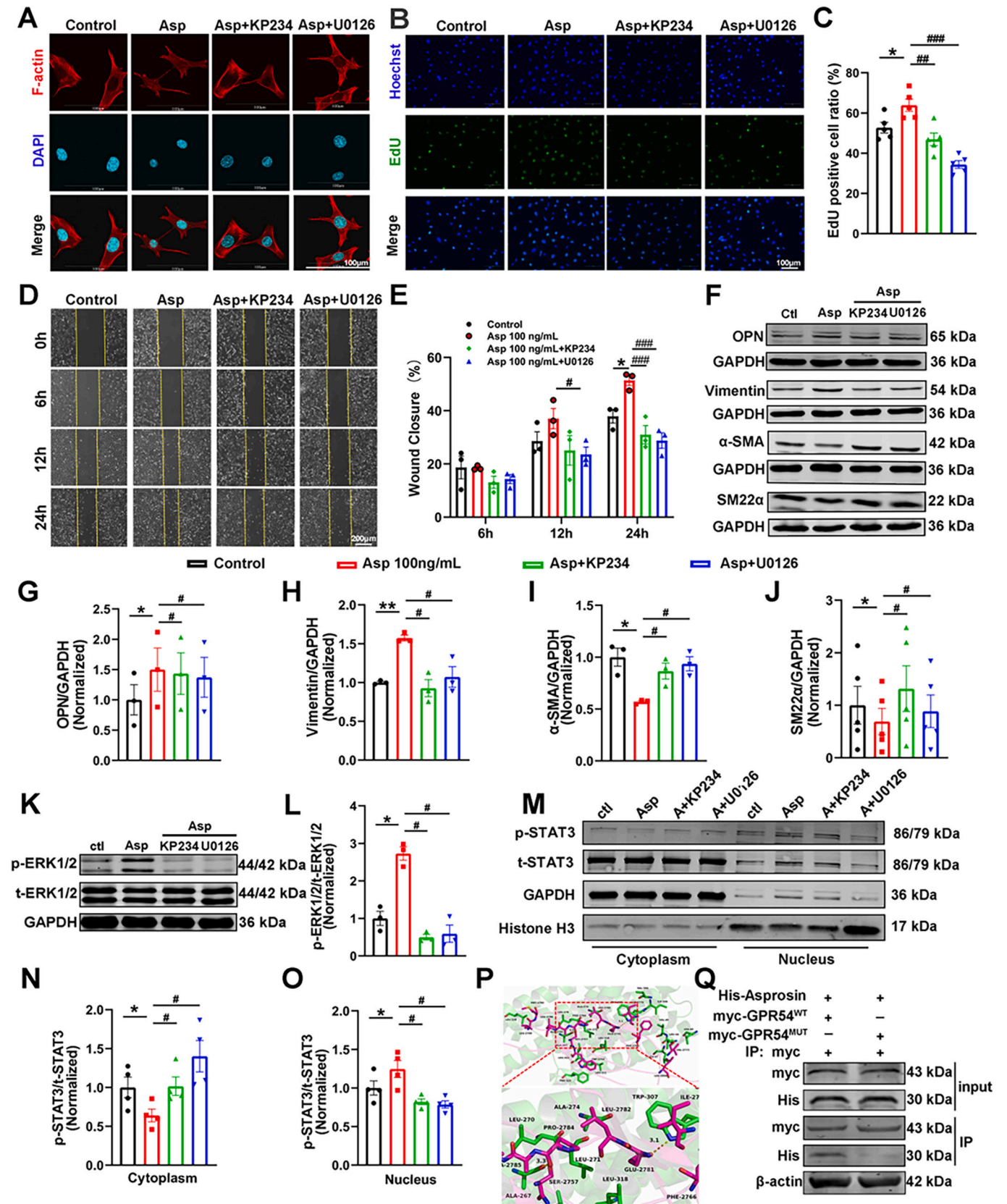
To prove whether asprosin induce VSMCs transformation from contractile phenotype to synthetic phenotype via GPR54 and Gαq/11, MOVAs pre-infected with scramble small interfering RNA (Si NC), GPR54 SiRNA or Gαq/11 SiRNA for 24 h, and then treated with 100 ng/ml asprosin. The Gαq/11 silencing efficiency was detected by qPCR and western blot (Fig. S7A-D). In the wound scratch assays, 100 ng/ml asprosin treatment time-dependently induced the increase of MOVAs migration, which was partially inhibited by silencing GPR54 or Gαq/11 (Fig. 6A, C). Results of EdU assay showed that asprosin treatment increased EdU positive cells, promoted cell proliferation, which were also partially inhibited by GPR54 SiRNA or Gαq/11 SiRNA (Fig. 6B, D). In addition, silencing GPR54 or Gαq/11 inhibited the increase in synthetic phenotype proteins OPN and Vimentin induced by asprosin treatment (Fig. 6E-G). Similarly, silencing treatment inhibited the decrease in contractile phenotype proteins α-SMA and SM22α induced by asprosin treatment (Fig. 6G, I, J). Moreover, GPR54 SiRNA or Gαq/11 SiRNA partially inhibited the activation of PLC, PKC and ERK1/2 (Fig. 6H, K, L, M).

3.7. GPR54 antagonist KP234 and ERK inhibitor U0126 attenuate asprosin induced phenotype transformation in MOVAs

To further prove whether asprosin induce MOVAs phenotype transformation via GPR54 and intracellular MAPKs signaling pathway, we treated MOVAs with GPR54 antagonist KP234 and MEK/ERK inhibitor U0126 in the presence of 100 ng/ml asprosin. As expected, phalloidin staining demonstrated KP234 and U0126 reversed asprosin induced F-actin reduction (Fig. 7A) and EdU assay showed that asprosin increased EdU positive cells, which was partially inhibited by KP234 or U0126 (Fig. 7B, C). KP234 or U0126 partially inhibited cell migration induced by asprosin (Fig. 7D, E). KP234 or U0126 also inhibited changes in proteins associated with phenotype transformation induced by asprosin (Fig. 7F-J). Similarly, we found that 2 μM KP234 and 10 μM U0126 significantly inhibited the activation of ERK1/2 (Fig. 7K, L). In addition, they inhibited STAT3 activation and nuclear translocation induced by asprosin (Fig. 7M-O). Molecular docking showed detailed structure analysis: two hydrogen bond interactions were shown between the residue Ala-267 of the GPR54 and the residue Ser-2757 of the asprosin (bond length: 3.3 Å), the residue Trp-307 of the GPR54 and the residue Glu-2781 of the asprosin (bond lengths: 3.1 Å), which formed the main binding affinity between the GPR54 and asprosin (Fig. 7P). Therefore, we designed plasmid simultaneous mutations of GPR54 protein residues Ala-267 and Trp-307 (Ala-267 mutated to Val-267 and Trp-307 mutated to Ala-307). The mutant plasmids were transfected into MOVAs, and COIP experiments were conducted to verify the interaction between asprosin and GPR54. The results showed that the mutant GPR54-(267, 307) residue cancelled the binding of asprosin and GPR54 (Fig. 7Q). GPR54 was knocked down in MOVAs, and on this basis, GPR54^{WT} and GPR54^{MUT} plasmids were overexpressed to detect the effect of asprosin induced phenotype transformation. The results of immunofluorescence showed that the mutant GPR54-(267, 307) inhibited asprosin induced MOVAs phenotype transformation (Fig. S8). These results indicate that asprosin induces MOVAs phenotype transformation via binding to GPR54-(267, 307) and recruiting Gαq/11, then activates the intracellular ERK1/2-STAT3 signaling pathway.

3.8. Asprosin antibody relieves atherosclerosis in ApoE^{-/-} mice

To determine whether asprosin antibody play a role in the treatment of atherosclerosis, ApoE^{-/-} mice were injected through tail vein with asprosin antibody once a week for 14 weeks starting from the 4th week of high-fat diet feeding (Fig. 8A). We detected the plasma asprosin level, as shown in Fig. 8B, we found that plasma asprosin decreased after administration of asprosin antibody. Western blot showed that asprosin antibody reduced asprosin level enriched to vascular smooth muscle (Fig. 8C, D). These results confirmed the successful injection of asprosin antibody. Furthermore, exogenous asprosin or asprosin antibody did not change asprosin level in adipose (Fig. S9). This indicates that exogenous recombinant asprosin or asprosin antibody do not affect the generation of endogenous asprosin. Next, we detected aortic diameter and blood flow by doppler ultrasound to evaluate vascular stiffness. Asprosin antibody treatment significantly increased the difference of diastolic and



(caption on next page)

Fig. 7. GPR54 antagonist KP234 and ERK inhibitor U0126 attenuate asprosin induced phenotype transformation in MOVAs. (A) Representative phalloidin staining of MOVAs treated by Asprosin (100 ng/ml), Asprosin+KP234 (2 μ M), Asprosin+U0126 (10 μ M). (B, C) Representative images and statistical data showed proliferation of MOVAs induced by Asprosin (100 ng/ml), Asprosin+KP234 (2 μ M), Asprosin+U0126 (10 μ M), $n = 5$ in each group. $^*P < 0.05$ vs. Control. $^{##}P < 0.05$ vs. Asprosin. $^{###}P < 0.01$ vs. Asprosin. (D, E) Representative images showed migration of MOVAs treated by Asprosin (100 ng/ml), Asprosin+KP234 (2 μ M), Asprosin+U0126 (10 μ M) at the time 0 h, 6 h, 12 h and 24 h measured by wound scratch assays. $n = 3$, $^*P < 0.05$ vs. Control. $^{###}P < 0.001$ vs. Asprosin. (F) Representative synthetic marker and contractile marker protein of MOVAs treated by Asprosin (100 ng/ml), Asprosin+KP234 (2 μ M), Asprosin+U0126 (10 μ M). (G, H) Synthetic marker OPN and Vimentin protein statistical data of MOVAs treated by Asprosin (100 ng/ml), Asprosin+KP234 (2 μ M), Asprosin+U0126 (10 μ M), $n = 3$ in each group, $^*P < 0.05$ vs. Control. $^{**}P < 0.05$ vs. Control. $^{#}P < 0.05$ vs. Asprosin. (I, J) Contractile marker α -SMA and SM22 α protein quantification data of MOVAs treated by Asprosin (100 ng/ml), Asprosin+KP234 (2 μ M), Asprosin+U0126 (10 μ M), $n = 3$ or 5 in each group, $^*P < 0.05$ vs. Control. $^{#}P < 0.05$ vs. Asprosin. (K, L) Representative p/t-ERK1/2 protein and quantification data of MOVAs treated by Asprosin (100 ng/ml), Asprosin+KP234 (2 μ M), Asprosin+U0126 (10 μ M), $n = 3$, $^*P < 0.05$ vs. Control. $^{#}P < 0.05$ vs. Asprosin. (M, N, O) Representative images and statistical data of nuclear and cytoplasmic p/t-STAT3 protein expression in MOVAs treated by Asprosin (100 ng/ml), Asprosin+KP234 (2 μ M), Asprosin+U0126 (10 μ M), $n = 4$, $^*P < 0.05$ vs. Control. $^{#}P < 0.05$ vs. Asprosin. (P) The molecular docking demonstrated the interaction between the GPR54 (green) and the asprosin (rose red). (Q) Co-immunoprecipitation demonstrated mutant GPR54-(267, 307) failed to combined with His-Asprosin in MOVAs. All data were shown as mean \pm SEM.

systolic diameter in aortic outflow tract and aortic arch (Fig. 8E, F, H). In addition, the results suggested that asprosin antibody significantly increased the forward/reverse flow ratio, indicating asprosin antibody decreased reverse flow (Fig. 8G, I). Combined with blood pressure data (Table S2), we calculated elastic modulus, stiffness index, and distensibility. These results suggested asprosin antibody reduced the elastic modulus, stiffness index and increased the distensibility in aortic outflow tract and aortic arch (Fig. 8J-L). These data demonstrated asprosin antibody restored vascular dysfunction caused by high fat diet to some extent.

We further examined the effect of asprosin antibody on plaque formation. Oil red O staining of aorta showed that asprosin antibody reduced the plaque area in aorta (Fig. 8M, N). Asprosin antibody inhibited lipid deposition (Fig. 8M, O, P) and reduced collagen content (Fig. 8M, Q) in aorta root. Besides, we examined the blood lipid levels, including TC, TG, LDL, and HDL, and found that recombinant asprosin increased plasma TG levels but did not affect other lipid levels, asprosin antibody failed to change lipid levels (Fig. S10). Asprosin antibody reduced the asprosin enriched to vascular smooth muscle (Fig. 8R, T). We next examined the effect of asprosin on VSMCs phenotype transformation in ApoE^{-/-} mice. As expected, the immunofluorescence staining showed that asprosin antibody inhibited the phenotype transformation in VSMCs (Fig. 8S, U, V). We used immunofluorescence to assess whether asprosin antibody reduced the co-localization of asprosin and GPR54 in vivo. According to the results, asprosin antibody not only decreased asprosin enrichment in the smooth muscle layer, but also lowered asprosin and GPR54 co-localization in aortic smooth muscle of ApoE^{-/-} mice (Fig. 8W). Co-immunoprecipitation results showed that asprosin antibody reduced the binding of asprosin to GPR54 in aorta compared with IgG antibody (Fig. 8X, Y).

4. Discussion

Phenotype transformation of VSMCs is an important pathological process in the occurrence and development of atherosclerosis. Under pathological conditions such as inflammation, hypertension, and diabetes, the proliferation and migration ability of VSMCs are significantly enhanced, and a large amount of extracellular matrix is synthesized, which is called synthetic VSMCs [33]. Inhibition of VSMCs proliferation and migration can alleviate the progress of atherosclerosis. Over the past 30 years, the molecular mechanisms of atherosclerosis have been extensively studied, and statins based lipid-regulating drugs have been shown to be the most effective medicine for the prevention and treatment of atherosclerosis [34]. With the clinical application of PCSK9 inhibitors, the regulation of blood lipids is becoming more stable [35,36]. However, there is still lack of treatment methods for other links in the pathogenesis and progression of atherosclerosis, such as phenotype transformation of VSMCs. Therefore, clarifying the influencing factors and mechanism of VSMCs phenotype transformation is of great significance. Our findings suggested that asprosin secreted by adipose aggravated atherosclerosis through promoting VSMCs transformation

from contractile phenotype to synthetic phenotype, while Asp^{KD} or asprosin antibody inhibited this process. Further work proved that asprosin promoted VSMCs phenotype transformation through binding to GPR54, coupling G α q/11 and activating the intracellular ERK1/2-STAT3 signaling pathway in VSMCs. Therefore, asprosin may be a novel progression predictor and therapeutic target of atherosclerosis.

Asprosin is mainly secreted by white adipose. Plasma asprosin level increases in both obesity mouse model and obese patients and children [37,38]. Previous research found that there was a strong positive association between asprosin level and triglycerides in T2DM patients [39]. As shown in Fig. S10, exogenous injection of asprosin increased plasma TG levels in atherosclerosis mice but failed to affect other lipid levels in our experiments, which is consistent with existing findings. Additionally, Qianqian Huang et al. reported that recombinant asprosin significantly increased the circulating levels of IL-6 and TNF- α and enhanced the adhesion of macrophages to endothelia characterized by the expression increase of CD68, ICAM-1, and VCAM-1 in rats [40]. Asprosin impaired insulin secretion through inducing the phosphorylation of protein kinase C- δ (PKC δ), eukaryotic initiation factor 2 (eIF2 α), and CHOP expression and inflammatory markers [14]. These works demonstrate the pro-inflammation effect of asprosin. Since the formation and retention of lipid-loaded macrophages in the lesion regions exacerbates atherosclerosis, and inflammation is an important pathological process in the development of atherosclerosis [41,42], we speculate that asprosin may promote the progression of atherosclerosis. However, the protective role of asprosin on atherosclerosis was also reported that asprosin inhibited lipid-loaded macrophage accumulation and reduces atherosclerotic burden by up-regulating ABCA1 and ABCG1 expression via the p38/Elk-1 pathway [43]. These research works indicate that asprosin participates in the regulation of blood lipids, vascular inflammatory response and may play complex roles in the occurrence and progress of atherosclerosis. In this study, we mainly observed the direct effect of asprosin on vascular, especially on the phenotype transformation of VSMCs from contractile phenotype to synthetic phenotype. Our data proves that asprosin promotes VSMCs transformation from contractile phenotype to synthetic phenotype, while Asp^{KD} or asprosin antibody inhibits this effect. We also detected the effect of asprosin on plaque formation and found that exogenous asprosin supplementation increased plaque area in ApoE^{-/-} mice (Fig. 2M, N), which was inhibited by Asp^{KD} (Fig. 3N, Q) and asprosin antibody (Fig. 8M, N). In addition, aortic root plaque lipid deposition and lesion area assessment suggested that asprosin promoted the formation of plaque (Fig. 2M, O, P), Asp^{KD} (Fig. 3O, R, S) and asprosin antibody inhibited this effect (Fig. 8M, O, P). Our results indicate that asprosin promotes pathological processes of atherosclerosis. Atherosclerosis is a complex pathological process. A variety of factors and several cell types are involved. The same factor may play disparate roles in different cell types and stages of atherosclerosis. Different researches usually focus on one aspect of this complicated process, and may obtain contradictory results. Researches about asprosin suggest that it plays different roles on different cell types and may affect different

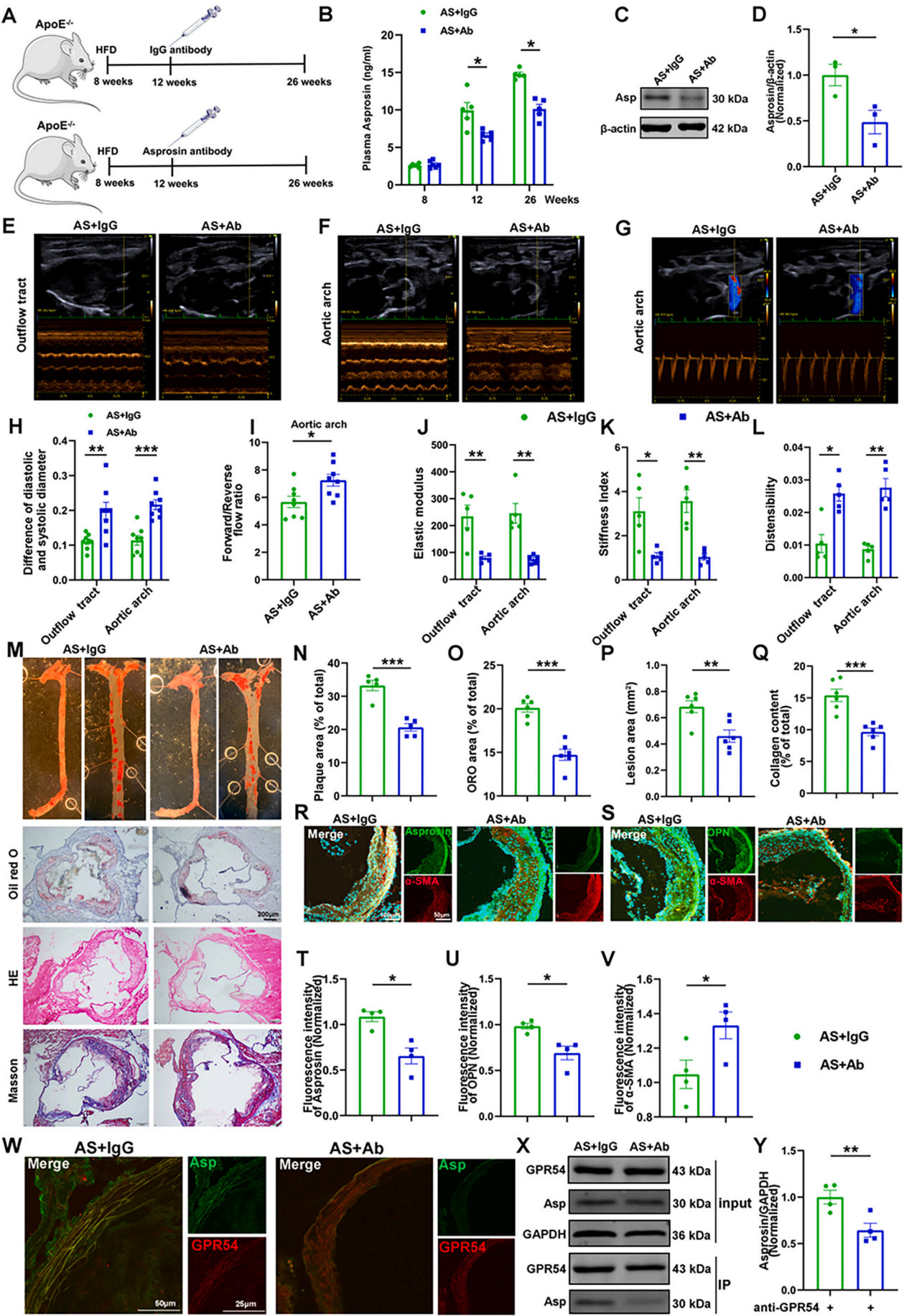


Fig. 8. Asprosin antibody relieves atherosclerosis. (A) Pattern diagram of tail vein administration of asprosin antibody in mice. (B) Plasma asprosin levels at different time points. $n = 5$ or 6 , $^*P < 0.05$ vs. (AS+IgG). (C, D) Representative western blot and quantification data of asprosin protein levels in aorta. $n = 3$, $^*P < 0.05$ vs. (AS+IgG). (E, F, H) Representative ultrasound images of aortic outflow tract and aortic arch and summarized data of the difference of diastolic and systolic diameter. IgG (IgG antibody, $15.56 \mu\text{g}\cdot\text{kg}^{-1}$), Ab (Asprosin antibody, $15.56 \mu\text{g}\cdot\text{kg}^{-1}$). $n = 8$, $^{**}P < 0.01$ vs. (AS+IgG), $^{***}P < 0.001$ vs. (AS+IgG). (G, I) Representative images of aortic arch flow and analyzed data of forward/reverse flow ratio. $n = 8$, $^*P < 0.05$ vs. (AS+IgG). (J, K, L) Summarized data of elastic modulus, stiffness index, and distensibility of aortic outflow tract and aortic arch. $n = 5$, $^*P < 0.05$ vs. (AS+IgG), $^{**}P < 0.01$ vs. (AS+IgG). (M) Representative Oil red O staining of aorta, aorta root and representative HE staining, masson staining of aorta root. (N) Summarized data of Oil red O staining of aorta. $n = 5$, $^{***}P < 0.001$ vs. (AS+IgG). (O) Summarized data of Oil red O staining of aorta root. $n = 6$, $^{***}P < 0.001$ vs. (AS+IgG). (P) Summarized HE staining of aorta root and summarized data. $n = 6$, $^{**}P < 0.01$ vs. (AS+IgG). (Q) Summarized masson staining of aorta root and summarized data. $n = 6$, $^{***}P < 0.001$ vs. (AS+IgG). (R, T) Representative immunofluorescence images of asprosin and α -SMA colocalization in aortic root. $n = 4$, $^*P < 0.05$ vs. (AS+IgG). (S, U, V) Representative immunofluorescence images of OPN and α -SMA double dyeing in aortic root. $n = 4$, $^*P < 0.05$ vs. (AS+IgG). (W) Representative immunofluorescence images of asprosin and GPR54 colocalization in aortic root. All data were shown as mean \pm SEM. (X, Y) Co-immunoprecipitation and statistical images in mice aorta of (AS+IgG) and (AS+Ab), it demonstrated asprosin antibody reduced combination of GPR54 and asprosin. The amount of anti-GPR54 was $15 \mu\text{g}$. $n = 4$, $^{**}P < 0.01$ vs. AS+IgG. All data were shown as mean \pm SEM.

pathological processes in the development of atherosclerosis. Our work concentrates on the changing of vascular smooth muscle cells in atherosclerosis progression, and prove asprosin aggravates atherosclerosis via regulating the phenotype transformation of vascular smooth muscle cells.

GPR54 is a classic GPCR, which was reported as an orphan receptor in rats. Until 2001, it has been found that GPR54 could specifically bind with Kiss1 encodes Kisspeptins (KPs), which is currently known as a ligand of GPR54 [44]. Among these KPs, KP-10 is a KP with the smallest molecular weight in the active form. It has been reported that KP-10 stimulates osteoblast differentiation through GPR54 mediated BMP2 expression regulation [45]. Some studies have showed that KP/GPR54 plays an important role in cell proliferation, migration and invasion. KP-10 regulated the proliferation of the rhesus monkey-derived stem cell line R366.4 [46]. Kisspeptin induced glioblastoma cell invasiveness via the KISS1R-Gq-PLC-PKC signaling pathway, while KISS1R siRNAs blocked kisspeptin-induced glioblastoma cell invasiveness [47]. Yanwei Li et al. reported KP-10 promoted bovine mammary epithelial cell proliferation by activating GPR54, AKT/mTOR/4EBP1 and ERK1/2/4EBP1 signaling pathways [48]. However, there are also different research reports about the effect of KP/GPR54 to cell migration. K Tan et al. reported Kiss1-induced GPR54 signaling inhibits breast cancer cell migration [49]. Victor A. reported that KP/GPR54 inhibited first trimester trophoblast cells invasion via inhibition of cell migration [50]. In addition, KP-54/GPR54 was found significantly increased in pancreatic catheter adenocarcinoma and Kiss1 overexpression inhibited tumor metastasis [51]. Therefore, GPR54 mediated cell proliferation, migration and invasion may vary according to different cell types. Most studies on the regulation of cell invasion and migration mediated by GPR54 activation focus on tumor cells. In our study, we found that activation of GPR54 promoted the proliferation and migration of vascular smooth muscle cells (Fig. S5), which plays an important role in phenotype transformation of VSMCs. Additionally, GPR54 couples with G α q/11, which is a G protein that binds and hydrolyzes guanosine 5'-triphosphate (GTP) to mediate downstream signaling [30,52]. Although asprosin does not affect GPR54 protein levels, it binds to GPR54, promotes the recruitment of G α q/11 to GPR54 and further activates intracellular ERK1/2-STAT3 signaling pathway in MOVAs.

KP/GPR54 binds G α q/11 to activate PLC, a family of membrane-associated enzymes that catalyze the decomposition of PIP2 to produce two important second messengers, IP3 and DAG, which regulate various cellular processes and serve as substrates for the synthesis of other important signaling molecules [53]. It has been widely proven that PLC activate PKC and MAPKs cascade (involving ERK and p38), further regulate the expression of corresponding proteins and affect biological or pathological processes in living system [54,55]. In VSMCs, activation of MAPKs signaling pathway promotes proliferation, migration and phenotype transformation [56]. STAT3 is a transcription activator, which is involved in various biological processes such as cell proliferation, survival, differentiation and angiogenesis [57]. After activation, p-STAT3 shifts to the nucleus and forms a complex with co activators in the nucleus, which binds to the promoter region of the target genes to

regulate their transcription [20]. Our work confirmed the effect of this signaling pathway in MOVAs. Asprosin increased PLC/PKC phosphorylation, which was attenuated by Si GPR54, GPR54 antagonist KP234 or Si G α q/11 treatment. GPR54 antagonist KP234 or ERK inhibitor U0126 attenuate asprosin-induced ERK1/2-STAT3 signal cascade and phenotype transformation respectively. To conclude, we have proved that asprosin induces phenotype transformation from contractile phenotype to synthetic phenotype in MOVAs through binding to GPR54, promoting the recruitment of G α q/11 to GPR54 and further activating intracellular PLC-PKC-ERK1/2-STAT3 signaling pathway in MOVAs. There has been report that GPR54 regulates ERK1/2 activity and hypothalamic gene expression in a G α q/11 and β -Arrestin-2 co-dependent manner [32]. Therefore, in addition to G α q/11, whether other downstream signal cascade is involved in the regulation of biological process after asprosin binding to GPR54 remains to be further studied. We did not further investigate the conformational changes following the activation of GPR54, which was a limitation of the present study.

5. Conclusions

This study proves that asprosin promotes the progress of atherosclerosis by inducing the transformation of VSMCs from contractile phenotype to synthetic phenotype, additionally, activating the GPR54/G α q/11-dependent ERK1/2-STAT3 signaling pathway in VSMCs to induce phenotype transformation of VSMCs is the key molecule mechanism for asprosin to promote the liability of blood vessels to atherosclerosis. Asp^{KD} in adipose tissue or treatment of asprosin antibody partially inhibits its effect. Although the understanding to asprosin is limited, and it is possible that many aspects of its physiological and pathophysiological activity remain to be discovered, our work reveals that asprosin may be a promising target to combat atherosclerosis by using anti-asprosin antibody or small molecular GPR54 signaling pathway inhibitors.

CRedit authorship contribution statement

Yu Zhao: Project administration, Writing – review & editing, Visualization. **Zhengkai Wang:** Investigation. **Yi Chen:** Investigation, Data curation. **Min Feng:** Conceptualization. **Xinxin Liu:** Investigation. **Huan Chen:** Investigation. **Nannan Wang:** Data curation. **Zhiqi Wang:** Data curation. **Shifeng Cao:** Investigation. **Jing Ren:** Formal analysis. **Xue Liu:** Methodology. **Yixiu Zhao:** Writing – review & editing, Project administration. **Yan Zhang:** Funding acquisition.

Declaration of competing interest

The authors declare that they have no known competing financial interests or personal relationships that could have appeared to influence the work reported in this paper.

Acknowledgments

This work was supported by the National Natural Science Foundation of China (82170431, 82330011, U21A20339, 82074148), the CAMS Innovation Fund for Medical Sciences (CIFMS, 2020-I2M-5-003).

Appendix A. Supplementary data

Supplementary data to this article can be found online at <https://doi.org/10.1016/j.ijbiomac.2024.131868>.

References

- [1] Y. Shang, C. Ma, J. Zhang, Z. Wang, C. Ren, X. Luo, R. Peng, J. Liu, J. Mao, Y. Shi, G. Fan, Bifunctional supramolecular nanofiber inhibits atherosclerosis by enhancing plaque stability and anti-inflammation in apoE(−/−) mice, *Theranostics* 10 (22) (2020) 10231–10244.
- [2] X.Y. Qi, S.L. Qu, W.H. Xiong, O. Rom, L. Chang, Z.S. Jiang, Perivascular adipose tissue (PVAT) in atherosclerosis: a double-edged sword, *Cardiovasc. Diabetol.* 17 (1) (2018) 134.
- [3] C. Romere, C. Duerschmid, J. Bournat, P. Constable, M. Jain, F. Xia, P.K. Saha, M. Del Solar, B. Zhu, B. York, P. Sarkar, D.A. Rendon, M.W. Gaber, S.A. LeMaire, J. S. Coselli, D.M. Milewicz, V.R. Sutton, N.F. Butte, D.D. Moore, A.R. Chopra, Asprosin, a fasting-induced glucogenic protein hormone, *Cell* 165 (3) (2016) 566–579.
- [4] X. Deng, Z. Zhao, L. Zhao, C. Wang, Y. Li, Z. Cai, H. Li, T. Gu, Y. Xia, Z. Zhang, D. Wang, L. Yang, G. Yuan, Association between circulating asprosin levels and carotid atherosclerotic plaque in patients with type 2 diabetes, *Clin. Biochem.* 109–110 (2022) 44–50.
- [5] M.L. Muthu, D.P. Reinhardt, Fibrillin-1 and fibrillin-1-derived asprosin in adipose tissue function and metabolic disorders, *Journal of cell communication and signaling* 14 (2) (2020) 159–173.
- [6] Y. Wang, H. Qu, X. Xiong, Y. Qiu, Y. Liao, Y. Chen, Y. Zheng, H. Zheng, Plasma Asprosin concentrations are increased in individuals with glucose dysregulation and correlated with insulin resistance and first-phase insulin secretion, *Mediators Inflamm.* 2018 (2018) 9471583.
- [7] J.H. Campbell, G.R. Campbell, Endothelial cell influences on vascular smooth muscle phenotype, *Annu. Rev. Physiol.* 48 (1986) 295–306.
- [8] M.R. Bennett, S. Sinha, G.K. Owens, Vascular smooth muscle cells in atherosclerosis, *Circ. Res.* 118 (4) (2016) 692–702.
- [9] E.M. Rzuclido, K.A. Martin, R.J. Powell, Regulation of vascular smooth muscle cell differentiation, *J. Vasc. Surg.* 45 Suppl A (2007) A25–A32.
- [10] J. Shi, Y. Yang, A. Cheng, G. Xu, F. He, Metabolism of vascular smooth muscle cells in vascular diseases, *American journal of physiology, Heart and circulatory physiology* 319 (3) (2020) H613–h631.
- [11] C. Mao, Z. Ma, Y. Jia, W. Li, N. Xie, G. Zhao, B. Ma, F. Yu, J. Sun, Y. Zhou, Q. Cui, Y. Fu, W. Kong, Nidogen-2 maintains the contractile phenotype of vascular smooth muscle cells and prevents neointima formation via bridging Jagged1-Notch3 signaling, *Circulation* 144 (15) (2021) 1244–1261.
- [12] F. Li, M. Jiang, M. Ma, X. Chen, Y. Zhang, Y. Zhang, Y. Yu, Y. Cui, J. Chen, H. Zhao, Z. Sun, D. Dong, Anthelmintics nitazoxanide protects against experimental hyperlipidemia and hepatic steatosis in hamsters and mice, *Acta Pharm. Sin. B* 12 (3) (2022) 1322–1338.
- [13] D.D. Zhang, Y. Song, P. Kong, X. Xu, Y.K. Gao, Y.Q. Dou, L. Weng, X.W. Wang, Y. L. Lin, F. Zhang, H. Zhang, M. Han, Smooth muscle 22 alpha protein inhibits VSMC foam cell formation by supporting normal LXRα signaling, ameliorating atherosclerosis, *Cell Death Dis.* 12 (11) (2021) 982.
- [14] M.A. Ovali, I. Bozgeyik, Asprosin, a C-terminal cleavage product of Fibrillin 1 encoded by the FBN1 gene, *Health and Disease, Mol Syndromol* 13 (3) (2022) 175–183.
- [15] J.L. Cavalcante, J.A. Lima, A. Redheuil, M.H. Al-Mallah, Aortic stiffness: current understanding and future directions, *J. Am. Coll. Cardiol.* 57 (14) (2011) 1511–1522.
- [16] J. Hashimoto, S. Ito, Aortic Blood Flow Reversal Determines Renal Function: Potential Explanation for Renal Dysfunction Caused by Aortic Stiffening in Hypertension, *Hypertension (Dallas, Tex. : 1979) vol. 66(1)*, 2015, pp. 61–67.
- [17] H.Y. Tang, A.Q. Chen, H. Zhang, X.F. Gao, X.Q. Kong, J.J. Zhang, Vascular smooth muscle cells phenotypic switching in cardiovascular diseases, *Cells* 11 (24) (2022).
- [18] Q. Yu, W. Li, R. Jin, S. Yu, D. Xie, X. Zheng, W. Zhong, X. Cheng, S. Hu, M. Li, Q. Zheng, G. Li, Z. Song, PI3Kγ (phosphoinositide 3-kinase γ) regulates vascular smooth muscle cell phenotypic modulation and Neointimal formation through CREB (cyclic AMP-response element binding protein)/YAP (yes-associated protein) signaling, *Arterioscler. Thromb. Vasc. Biol.* 39 (3) (2019) e91–e105.
- [19] N. Lédard, A. Liboz, B. Blondeau, M. Babiak, C. Moulin, B. Vallin, I. Guillas, V. Mateo, C. Jumeau, K. Bliando, O. Meilhac, I. Limon, M. Glorian, Slug, a Cancer-related transcription factor, is involved in vascular smooth muscle cell Transdifferentiation induced by platelet-derived growth factor-BB during atherosclerosis, *J. Am. Heart Assoc.* 9 (2) (2020) e014276.
- [20] X.H. Liao, N. Wang, D.W. Zhao, D.L. Zheng, L. Zheng, W.J. Xing, W.J. Ma, L.Y. Bao, J. Dong, T.C. Zhang, STAT3 protein regulates vascular smooth muscle cell phenotypic switch by interaction with Myocardin, *J. Biol. Chem.* 290 (32) (2015) 19641–19652.
- [21] X. Tang, Y. Liu, Q. Xiao, Q. Yao, M. Allen, Y. Wang, L. Gao, Y. Qi, P. Zhang, Pathological cyclic strain promotes proliferation of vascular smooth muscle cells via the ACTH/ERK/STAT3 pathway, *J. Cell. Biochem.* 119 (10) (2018) 8260–8270.
- [22] S.B. Lee, W.S. Lee, J.S. Shin, D.S. Jang, K.T. Lee, Xanthotoxin suppresses LPS-induced expression of iNOS, COX-2, TNF-α, and IL-6 via AP-1, NF-κB, and JAK-STAT inactivation in RAW 264.7 macrophages, *Int. Immunopharmacol.* 49 (2017) 21–29.
- [23] D. Qin, L. Zhang, X. Jin, Z. Zhao, Y. Jiang, Z. Meng, Effect of Endothelin-1 on proliferation, migration and fibrogenic gene expression in human RPE cells, *Peptides* 94 (2017) 43–48.
- [24] A. Breit, V. Besik, H.J. Solinski, S. Muehlich, E. Glas, S.J. Yarwood, T. Gudermann, Serine-727 phosphorylation activates hypothalamic STAT-3 independently from tyrosine-705 phosphorylation, *Molecular endocrinology (Baltimore, Md.)* 29 (3) (2015) 445–459.
- [25] Y.F. Chen, K.J. Wu, L.R. Siao, H.Y. Tsai, Trilinolein, a natural triacylglycerol, protects cerebral ischemia through inhibition of neuronal apoptosis and ameliorates intimal hyperplasia via attenuation of migration and modulation of matrix Metalloproteinase-2 and RAS/MEK/ERK signaling pathway in VSMCs, *Int. J. Mol. Sci.* 23 (21) (2022).
- [26] E. Li, H. Shan, L. Chen, A. Long, Y. Zhang, Y. Liu, L. Jia, F. Wei, J. Han, T. Li, X. Liu, H. Deng, Y. Wang, OLF734 mediates glucose metabolism as a receptor of Asprosin, *Cell Metab.* 30 (2) (2019) 319–328.e8.
- [27] A. Wolfe, M.A. Hussain, The emerging role(s) for Kisspeptin in metabolism in mammals, *Front. Endocrinol. (Lausanne)* 9 (2018) 184.
- [28] T. Watanabe, K. Sato, Roles of the kisspeptin/GPR54 system in pathomechanisms of atherosclerosis, Nutrition, metabolism, and cardiovascular diseases : NMCD 30 (6) (2020) 889–895.
- [29] K. Sato, R. Shirai, M. Hontani, R. Shinooka, A. Hasegawa, T. Kichise, T. Yamashita, H. Yoshizawa, R. Watanabe, T.A. Matsuyama, H. Ishibashi-Ueda, S. Koba, Y. Kobayashi, T. Hirano, T. Watanabe, Potent vasoconstrictor Kisspeptin-10 induces atherosclerotic plaque progression and instability: reversal by its receptor GPR54 antagonist, *J. Am. Heart Assoc.* 6 (4) (2017).
- [30] F. Fratangelo, M.V. Carriero, M.L. Motti, Controversial role of Kisspeptins/KISS-1R signaling system in tumor development, *Front. Endocrinol. (Lausanne)* 9 (2018) 192.
- [31] J.P. Castano, A.J. Martinez-Fuentes, E. Gutierrez-Pascual, H. Vaudry, M. Tena-Sempere, M.M. Malagon, Intracellular signaling pathways activated by kisspeptins through GPR54: do multiple signals underlie function diversity? *Peptides* 30 (1) (2009) 10–15.
- [32] J.M. Szareszewski, M. Pampillo, M.R. Ahow, S. Offermanns, M. Bhattacharya, A. V. Babwah, GPR54 regulates ERK1/2 activity and hypothalamic gene expression in a Gαq/11 and β-arrestin-dependent manner, *PLoS One* 5 (9) (2010) e12964.
- [33] B.H. Lu, H.B. Liu, S.X. Guo, J. Zhang, D.X. Li, Z.G. Chen, F. Lin, G.A. Zhao, Long non-coding RNAs: modulators of phenotypic transformation in vascular smooth muscle cells, *Front. Cardiovasc. Med.* 9 (2022) 959955.
- [34] J. Fan, T. Watanabe, Atherosclerosis: known and unknown, *Pathol. Int.* 72 (3) (2022) 151–160.
- [35] A. Pasta, A.L. Cremonini, L. Pisciotta, A. Buscaglia, I. Porto, F. Barra, S. Ferrero, C. Brunelli, G.M. Rosa, PCSK9 inhibitors for treating hypercholesterolemia, *Expert Opin. Pharmacother.* 21 (3) (2020) 353–363.
- [36] N.G. Lintner, K.F. McClure, D. Petersen, A.T. Londregan, D.W. Piotrowski, L. Wei, J. Xiao, M. Bolt, P.M. Loria, B. Maguire, K.F. Geoghegan, A. Huang, T. Rolph, S. Liras, J.A. Doudna, R.G. Dullea, J.H. Cate, Selective stalling of human translation through small-molecule engagement of the ribosome nascent chain, *PLoS Biol.* 15 (3) (2017) e2001882.
- [37] C.Y. Wang, T.A. Lin, K.H. Liu, C.H. Liao, Y.Y. Liu, V.C. Wu, M.S. Wen, T.S. Yeh, Serum asprosin levels and bariatric surgery outcomes in obese adults, *Int. J. Obes. (Lond)* 43 (5) (2005) 1019–1025 (2019).
- [38] E. Sünnetçi Silistre, H.U. Hatipoğlu, Increased serum circulating asprosin levels in children with obesity, *Pediatrics international : official journal of the Japan Pediatric Society* 62 (4) (2020) 467–476.
- [39] L. Zhang, C. Chen, N. Zhou, Y. Fu, X. Cheng, Circulating asprosin concentrations are increased in type 2 diabetes mellitus and independently associated with fasting glucose and triglyceride, *Clinica chimica acta; international journal of clinical chemistry* 489 (2019) 183–188.
- [40] Q. Huang, S. Chen, X. Xiong, T. Yin, Y. Zhang, G. Zeng, Q. Huang, Asprosin exacerbates endothelium inflammation induced by hyperlipidemia through activating IKKβ-NF-κBp65 pathway, *Inflammation* 46 (2) (2023) 623–638.
- [41] S. Taleb, Inflammation in atherosclerosis, *Arch. Cardiovasc. Dis.* 109 (12) (2016) 708–715.
- [42] M.H. Ma, F.F. Li, W.F. Li, H. Zhao, M. Jiang, Y.Y. Yu, Y.C. Dong, Y.X. Zhang, P. Li, W.J. Bu, Z.J. Sun, D.L. Dong, Repurposing nitazoxanide as a novel anti-atherosclerotic drug based on mitochondrial uncoupling mechanisms, *Br. J. Pharmacol.* 180 (1) (2023) 62–79.
- [43] J. Zou, C. Xu, Z.W. Zhao, S.H. Yin, G. Wang, Asprosin inhibits macrophage lipid accumulation and reduces atherosclerotic burden by up-regulating ABCA1 and ABCG1 expression via the p38/Elk-1 pathway, *J. Transl. Med.* 20 (1) (2022) 337.
- [44] T. Ohtaki, Y. Shintani, S. Honda, H. Matsumoto, A. Hori, K. Kanehashi, Y. Terao, S. Kumano, Y. Takatsu, Y. Masuda, Y. Ishibashi, T. Watanabe, M. Asada, T. Yamada, M. Suenaga, C. Kitada, S. Usuki, T. Kurokawa, H. Onda, O. Nishimura, M. Fujino, Metastasis suppressor gene KISS-1 encodes peptide ligand of a G-protein-coupled receptor, *Nature* 411 (6837) (2001) 613–617.
- [45] H.E. Son, K.M. Kim, E.J. Kim, W.G. Jang, Kisspeptin-10 (KP-10) stimulates osteoblast differentiation through GPR54-mediated regulation of BMP2 expression and activation, *Sci. Rep.* 8 (1) (2018) 2134.

- [46] T. Huma, Z. Wang, J. Rizak, F. Ahmad, M. Shahab, Y. Ma, S. Yang, X. Hu, Kisspeptin-10 modulates the proliferation and differentiation of the rhesus monkey derived stem cell line: R366.4, *TheScientificWorldJournal* 2013 (2013) 135470.
- [47] S.G. Kim, J.Y. Sung, J.R. Kim, H.C. Choi, Quercetin-induced apoptosis ameliorates vascular smooth muscle cell senescence through AMP-activated protein kinase signaling pathway, *The Korean journal of physiology & pharmacology : official journal of the Korean Physiological Society and the Korean Society of Pharmacology* 24 (1) (2020) 69–79.
- [48] Y. Li, Y. Cao, J. Wang, S. Fu, J. Cheng, L. Ma, Q. Zhang, W. Guo, X. Kan, J. Liu, Kp-10 promotes bovine mammary epithelial cell proliferation by activating GPR54 and its downstream signaling pathways, *J. Cell. Physiol.* 235 (5) (2020) 4481–4493.
- [49] K. Tan, S.G. Cho, W. Luo, T. Yi, X. Wu, S. Siwko, M. Liu, W. Yuan, KiSS1-induced GPR54 signaling inhibits breast cancer cell migration and epithelial-mesenchymal transition via protein kinase D1, *Curr. Mol. Med.* 14 (5) (2014) 652–662.
- [50] V.A. Francis, A.B. Abera, M. Matjila, R.P. Millar, A.A. Katz, Kisspeptin regulation of genes involved in cell invasion and angiogenesis in first trimester human trophoblast cells, *PLoS One* 9 (6) (2014) e99680.
- [51] L.R. McNally, D.R. Welch, B.H. Beck, L.J. Stafford, J.W. Long, J.C. Sellers, Z. Q. Huang, W.E. Grizzle, C.R. Stockard, K.T. Nash, D.J. Buchsbaum, KiSS1 over-expression suppresses metastasis of pancreatic adenocarcinoma in a xenograft mouse model, *Clin. Exp. Metastasis* 27 (8) (2010) 591–600.
- [52] T.H. Kim, J.H. Yoon, S.G. Cho, Kisspeptin promotes glioblastoma cell invasiveness via the Gq-PLC-PKC pathway, *Anticancer Res* 40 (1) (2020) 213–220.
- [53] X. Liu, K. Lee, A.E. Herbison, Kisspeptin excites gonadotropin-releasing hormone neurons through a phospholipase C/calcium-dependent pathway regulating multiple ion channels, *Endocrinology* 149 (9) (2008) 4605–4614.
- [54] K. Hisano, H. Yoshida, S. Kawase, T. Mimura, H. Haniu, T. Tsukahara, T. Kurihara, Y. Matsuda, N. Saito, T. Uemura, Abundant oleoyl-lysophosphatidylethanolamine in brain stimulates neurite outgrowth and protects against glutamate toxicity in cultured cortical neurons, *J. Biochem.* 170 (3) (2021) 327–336.
- [55] G. Yi, S. Zhang, Y. Ma, X. Yang, F. Huo, Y. Chen, B. Yang, W. Tian, Matrix vesicles from dental follicle cells improve alveolar bone regeneration via activation of the PLC/PKC/MAPK pathway, *Stem Cell Res Ther* 13 (1) (2022) 41.
- [56] E.A. Rodriguez, GATA2 promotes human vascular smooth muscle cell proliferation via mitofusin2- mediated Ras/Raf/MEK/ERK signaling pathway. New target in vascular medicine, *International journal of cardiology* 353 (2022) 86–87.
- [57] N. Zhang, Y. Zhang, S. You, Y. Tian, S. Lu, L. Cao, Y. Sun, Septin4 prevents PDGF-BB-induced HAVSMC phenotypic transformation, proliferation and migration by promoting SIRT1-STAT3 deacetylation and dephosphorylation, *Int. J. Biol. Sci.* 16 (4) (2020) 708–718.